Targeting Lysosomes by Design: Novel *N*-Acridine Thiosemicarbazones that Enable Direct Detection of Intracellular Drug Localization and Overcome P-Glycoprotein (Pgp)-Mediated Resistance.

Busra Kaya,[1] Henry Smith,[1] Yanbing Chen,[1] Mahan Gholam Azad,[1,2] Tiffany M. Russell,[1] Vera Richardson,[1,2] Paul V. Bernhardt,[3] Mahendiran Dharmasivam,[1,2]* and Des R. Richardson,[1,2,4]*

[1]Centre for Cancer Cell Biology and Drug Discovery, Griffith University, Nathan, 4111, Australia; [2]Molecular Pharmacology and Pathology Program, Department of Pathology and Bosch Institute, University of Sydney, Sydney, New South Wales, Australia; [3]School of Chemistry and Molecular Biosciences, University of Queensland, Brisbane, 4072, Australia; [4]Department of Pathology and Biological Responses, Nagoya University Graduate School of Medicine, Nagoya 466-8550, Japan.

***Corresponding authors**: ***To whom correspondence should be addressed:** Dr. Des R. Richardson and Dr. M. Dharmasivam, Centre for Cancer Cell Biology and Drug Discovery, Griffith University, Nathan, Brisbane, 4111, Queensland, Australia. Email: d.richardson@griffith.edu.au; m.dharmasivam@griffith.edu.au

Table of Contents

Supplementary Procedures

Supplementary Tables

Supplementary Results and Discussion

Supplementary Figures

General methods

^{1}H and ^{13}C NMR spectra were recorded at 25 °C on a Bruker (Billerica, MA, USA) Avance III 800 MHz NMR spectrometer equipped with a cryoprobe using DMSO-d_6, or $CDCl_3$. A Thermo Scientific Flash 2000 CHNS/O analyzer (Waltham, MA) was used for the elemental analysis. LC-MS data were collected using a Thermo Fisher Ultimate 3000 RS LC-MS UHPLC-ISQ Single Quadrupole mass spectrometer (electrospray ionization; ESI). HR-MS data were collected using a Bruker MaXis UHR ESI QTOF mass spectrometer. Photoluminescence spectroscopy was conducted using a Lumina Fluorescence Spectrometer (Thermo Fisher; USA, MA).

Chemicals

9-Chloroacridine, KSCN, TBAB, 2-acetylpyridine, 2-acetylpyrazine, 2-benzoylpyridine, di(2-pyridyl) ketone, hydrazine monohydrate, triethylamine, DMSO-d_6, $CDCl_3$, $Fe(ClO_4)_3 \cdot 6H_2O$, $Cu(ClO_4)_2.6H_2O$, $Zn(ClO_4)_2 \cdot 6H_2O$, Doxorubicin hydrochloride, Desferrioxamine (DFO), MTT, skeletal muscle myoglobin (95–100% purity), and all solvents were acquired from Sigma-Aldrich (St. Louis, MO), at the highest analytical purity available.

General Synthesis

Dp44mT, DpC, PPP44mT, and $[Zn(DpC)_2]$ were synthesized and characterized by standard methods, as described previously.[1-5] The hydrazones (**1-4**) and 9-isothiocyanatoacridine were synthesized according to standard procedures[6-10] and structurally characterized by elemental analysis, LC-MS, and NMR.

Synthesis of the NAT Ligands

Step A: Hydrazones

An equivalent of ketone or aldehyde (1 *eq.*) was reacted with hydrazine monohydrate (3 *eq.*) in the minimum amount of EtOH required to dissolve the starting material at 70 °C. The reaction was refluxed for 5 h and stirred at room temperature for 12 h before drying *in vacuo* to remove excess EtOH. The reaction mixture was cooled to room temperature and put through aqueous extraction, with minimum H_2O and dichloromethane (DCM; 3 x 50 mL washes). The DCM layer with product was retained, neutralized, and dried with Na_2SO_4, before solvent removal by gentle, but thorough rotary evaporation to yield the hydrazone products as crystals.

(*E*)-2-(hydrazineylidene(phenyl)methyl)pyridine (1): This compound was prepared according to step A from 2-benzoylpyridine (5 g; 27.29 mmol) and hydrazine monohydrate (3 eq.; 4.1 mL). After thorough drying *in vacuo*, the product was obtained as white crystals (5.41 g). Yield: 98%. LC-MS (positive mode) m/z calcd. for $[C_{12}H_{11}N_3]$: 198.16 $[M + H]^+$. Found: 198.10. ^{1}H NMR ($CDCl_3$, 800 MHz): δ 8.51 (m, 1H), 7.68 (m, 1H), 7.59 (m, 1H), 7.49 (m, 2H), 7.40 (m, 1H), 7.30 (m. 2H), 7.10 (m, 1H), 5.71 (s, 2H). ^{13}C NMR ($CDCl_3$, 200 MHz): δ 156.31, 149.09, 147.82, 136.06, 132.26, 129.29, 129.01, 128.91, 122.28, 120.99.

2,2'-(hydrazineylidenemethylene)dipyridine (2): The agent was synthesized according to step A from di-2-pyridyl ketone (5 g, 27.14 mmol) and hydrazine monohydrate (3 eq, 4.1 mL). After thorough drying *in vacuo*, the product was obtained as white crystals (4.95 g). Yield 92%. LC-MS (positive mode) m/z calcd. for $[C_{11}H_{10}N_4]$: 199.09 $[M + H]^+$. Found: 199.20. ^{1}H NMR ($CDCl_3$, 800 MHz): δ 8.52 (m, 2H), 7.62 (m, 2H), 7.53 (m, 2H), 7.15 (m, 2H), 5.92 (s, 2H). ^{13}C NMR ($CDCl_3$, 200 MHz): δ 160.83, 148.19, 136.96, 122.63, 121.22, 75.30.

(*E*)-2-(1-hydrazineylideneethyl)pyrazine (3). The agent was synthesized according to step A from 2-acetylpyrazine (3.5 g; 28.65 mmol) and hydrazine monohydrate (3 eq.; 4.3 mL). After thorough drying *in vacuo*, product was obtained as white crystals (3.78 g). Yield: 97%. LC-MS (positive mode) m/z calcd. for $[C_6H_8N_4]$: 137.08 $[M + H]^+$. Found: 137.20. ^1H NMR ($CDCl_3$, 800 MHz): δ 9.16 (m, 1H), 8.40 (m, 1H), 8.35 (m, 1H), 5.77 (s, 2H), 2.17 (s, 3H). ^{13}C NMR ($CDCl_3$, 200 MHz): δ 151.83, 144.84, 142.68, 142.54, 142.40, 9.02.

(*E*)-2-(1-hydrazineylideneethyl)pyridine (4): The compound was prepared according to step A from 2-acetylpyridine (3.24 mL, 28.89 mmol) and hydrazine monohydrate (3 eq., 4.4 mL). After thorough drying *in vacuo*, the product was obtained as white crystals (3.82 g). Yield: 98%. LC-MS (positive mode) m/z calcd. for $[C_7H_9N_3]$: 136.08 $[M + H]^+$. Found: 136.20. ^1H NMR ($CDCl_3$, 800 MHz): δ 8.50 (m, 1H), 7.90 (m, 1H), 7.59 (m, 1H), 7.13 (m, 1H), 5.55 (s, 2H), 2.22 (s, 3H). ^{13}C NMR ($CDCl_3$, 200 MHz): δ 196.55, 148.37, 147.60, 136.06, 122.55, 119.74, 9.62.

Step B: 9-Isothiocyanatoacridine

9-chloroacridine (5 g; 21.1 mmol) and KSCN (3 g; 63.3 mmol) were added to 200 mL of acetone, along with tetrabutylammonium bromide (TBAB; 0.68 g; 2.11 mmol) as a phase transfer catalyst. The reaction was refluxed for 3 h and the mixture added to 100 mL of H_2O, before vacuum filtering to obtain the crude product. The crude compound was then crystallized in excess hot acetone (30 mL), before being cooled to 0 °C to yield 9-isothiocyanatoacridine, a yellow solid (4.78 g). Yield: 96%. LC-MS (positive mode) m/z calcd. for $[C_{14}H_8N_2S]$: 237.04 $[M + H]^+$. Found: 237.0. ^1H NMR ($CDCl_3$, 800 MHz): δ 8.18 (m, 4H), 7.78 (m, 2H), 7.59 (m, 2H). ^{13}C NMR ($CDCl_3$, 200 MHz): δ 149.19, 140.75, 132.80, 130.72, 129.80, 127.06. 122.96, 122.03.

Step C: NATs

9-Isothiocyanatoacridine (1 eq.) was added to a double-necked flask held in an ice bath at 0 °C, followed by 10 mL MeOH/gram of isothiocyanatoacridine. The mixture was allowed to cool, and the flask was sealed with a septum pierced by a needle before flushing the flask thoroughly with nitrogen. While continuing to flush the flask with N_2, excess of the relevant hydrazone (0.2 mmol) (**1-4**) in MeOH, cooled to 0 °C, was added by syringe through the septum. The reaction vessel was sealed and stirred at 0 °C for 2 h, and then gradually allowed to increase to room temperature, before stirring for 16 h. The resulting mixture was filtered over vacuum and washed thoroughly with methanol to obtain a beige to yellow powder.

(*E*)-N-(acridin-9-yl)-2-(phenyl(pyridin-2-yl)methylene)hydrazine-1-carbothioamide (AOBP): The compound was synthesized according to step C, from the reaction of isothiocyanatoacridine (4g, 17 mmol) with hydrazone **1** (3.39 g; 17.2 mmol). The product was obtained as a beige powder and recrystallized from MeOH to give AOBP as large orange-red crystals (6.55 g). Yield: 89%. HR-MS (positive mode) m/z calcd. for $[C_{26}H_{19}N_5S]$: 434.1434 $[M + H]^+$. Found: 434.1436. ^{1}H NMR (800 MHz, $CDCl_3$) δ 14.49 (s, 1H), 9.73 (s, 1H), 8.90 (d, J = 3.8 Hz, 1H), 8.25 (d, J = 8.5 Hz, 2H), 8.17 (d, J = 8.6 Hz, 2H), 7.85 (td, J = 7.9, 1.2 Hz, 1H), 7.81 – 7.74 (m, 2H), 7.65 (dd, J = 17.5, 6.6 Hz, 2H), 7.60 – 7.55 (m, 2H), 7.50 – 7.43 (m, 5H).^{13}C NMR ($CDCl_3$, 200 MHz): δ 179.29, 152.38, 149.68, 148.76, 143.86, 139.96, 137.51, 137.33, 136.78, 130.33, 130.00, 129.64, 129.30, 128.71, 126.70, 126.57, 124.68, 124.17, 123.83. Anal. calcd. for $C_{26}H_{19}N_5S$: C, 72.03; H, 4.42; N, 16.16; S, 7.40. Found: C, 72.29; H, 4.37; N, 16.24; S, 7.14.

***(E)-N*-(acridin-9-yl)-2-(di(pyridin-2-yl)methylene)hydrazine-1-carbothioamide (AODP):** The compound was prepared according to step C, from isothiocyanatoacridine (4 g; 17 mmol)

and hydrazone **2** (3.76 g; 19 mmol). The product was obtained as yellow-beige powder and recrystallized from MeCN to give orange-red crystals (5.2 g). Yield: 71%. HR-MS (positive mode) m/z calcd. for $[C_{25}H_{18}N_6S]$: 435.1386 $[M + H]^+$. Found: 435.1392. ^1H NMR (800 MHz, $CDCl_3$) δ 14.95 (s, 1H), 9.80 (s, 1H), 8.87 (d, *J* = 3.3 Hz, 1H), 8.69 (s, 1H), 8.26 (d, *J* = 8.5 Hz, 2H), 8.17 (d, *J* = 8.6 Hz, 2H), 7.90 – 7.77 (m, 5H), 7.62 – 7.59 (m, 1H), 7.59 – 7.55 (m, 2H), 7.47 – 7.43 (m, 1H), 7.39 (d, *J* = 5.1 Hz, 1H). ^{13}C NMR ($CDCl_3$, 200 MHz): δ 179.10, 155.78, 151.61, 149.64, 148.94, 148.23, 141.50, 139.85, 137.20, 130.32, 129.99, 127.04, 126.59, 124.61, 124.19, 124.10, 123.94, 123.76. Anal. calcd. for $C_{25}H_{18}N_6S$: C, 69.10; H, 4.18; N, 19.34; S, 7.38. Found: C, 68.98; H, 4.32; N, 19.33; S, 6.99.

(2E)-*N*-(acridin-9-yl)-2-[1-(pyrazin-2-yl)ethylidene]hydrazine-1-carbothioamide (AOAPZ). The agent was synthesized according to step C, from isothiocyanatoacridine (4 g; 17 mmol) and hydrazone **3** (2.56 g; 19 mmol). The product was obtained as a beige-white powder (6.19 g). Yield: 98%. HR-MS (positive mode) m/z calcd. for $[C_{20}H_{16}N_6S]$: 373.1229 $[M + H]^+$. Found: 373.1218. ^1H NMR (800 MHz, DMSO) δ 11.88, 11.16 (s, 1H), 11.05, 9.99 (s, 1H), 8.71(d, J = 36.6 Hz, 1H), 8.58 – 8.36 (m, 1H), 8.28 (d, J = 8.6 Hz, 1H), 8.19 (d, J = 20.2 Hz, 1H), 8.16 (d, J = 8.5 Hz, 1H), 7.93 (t, J = 7.3 Hz, 2H), 7.74 – 7.68 (m, 2H), 7.56 (d, J = 7.6 Hz, 1H), 7.28 (d, J = 6.3 Hz, 1H), 2.63, 2.42 (s, 3H). ^{13}C NMR (201 MHz, d_6-DMSO) δ 180.02, 150.43, 149.56, 148.25, 144.70, 144.16, 143.69, 142.91, 140.21, 133.45, 130.95, 129.75, 128.08, 126.67, 125.04, 124.56, 122.04, 117.63, 116.63, 12.89-12.39. Anal. calcd. for $[C_{20}H_{16}N_6S]$: C, 64.50; H, 4.33; N, 22.56; S, 8.61. Found: C, 64.54; H, 4.45; N, 22.23; S, 8.24.

(2E)-*N*-(acridin-9-yl)-2-[1-(pyridin-2-yl)ethylidene]hydrazine-1-carbothioamide (AOAP). The agent was prepared according to step C, from isothiocyanatoacridine (4g; 17 mmol) and **4** (2.56 g; 19 mmol). The product was obtained as a beige-white powder (6.11 g).

Yield: 97% yield. HR-MS (positive mode) m/z calcd. for $[C_{21}H_{17}N_5S]$: 372.1277 $[M + H]^+$. Found: 372.1263. ^1H NMR (800 MHz, DMSO) δ 11.74, 11.24 (s, 1H), 10.87, 9.97 (s, 1H), 8.71 – 8.62 (m, 1H), 8.22 (d, J = 8.7 Hz, 1H), 8.16 – 8.12 (m, 1H), 8.10 (d, J = 8.6 Hz, 1H), 7.90 – 7.85 (m, 1H), 7.78 (dd, J = 16.3, 9.1 Hz, 1H), 7.69 – 7.62 (m, 2H), 7.49 (d, J = 8.3 Hz, 1H), 7.43 – 7.40 (m, 1H), 7.28 – 7.19 (m, 2H), 2.59, 2.39 (s, 3H). 13C NMR (201 MHz, d_6-DMSO) δ 179.78, 155.00, 150.25, 149.52, 148.92, 146.22, 143.08, 140.11, 138.56, 136.75, 133.29, 130.82, 129.72, 127.74, 126.64, 125.05, 124.65, 121.75, 117.52, 116.72, 13.15-13.09. Anal. calcd. for $[C_{21}H_{17}N_5S]$: C, 67.90; H, 4.61; N, 18.85; S 8.63. Found: C, 67.85; H, 4.76; N, 18.71; S, 8.41.

General synthetic procedure of the Fe(III) complexes

The NATs (2 mmol) were dissolved in 20 mL of EtOH, and $Fe(ClO_4)_3.6H_2O$ (1 mmol) was added. The mixture was stirred for 20 min at room temperature and then Et_3N (1.1 mmol) was added. The precipitate was filtered off, washed with cold EtOH and Et_2O, and dried *in vacuo*.

[Fe(AOBP)$_2$](ClO$_4$)

AOBP (630 mg, 1.45 mmol), $Fe(ClO_4)_3.6H_2O$ (270 mg, 0.727 mmol) and Et_3N (0.11 g; 1.1 mmol) were used as reagents for the preparation of $[Fe(AOBP)_2](ClO_4)$. Dark brown powder (0.42 g). Yield: 57%. HR-MS (positive mode) m/z calcd. for $[C_{52}H_{36}FeN_{10}S_2]^+$: 920.1910 $[M - ClO_4]^+$. Found: 920.1906. Anal. calcd. for $[C_{52}H_{36}FeN_{10}S_2]\cdot(ClO_4)$: C, 61.21; H, 3.56; N, 13.73; S, 6.29. Found: C, 61.44; H, 3.35; N, 13.72; S, 6.27.

[Fe(AODP)$_2$](ClO$_4$)

AODP (614 mg, 1.4 mmol), $Fe(ClO_4)_3.6H_2O$ (263 mg; 0.707 mmol) and Et_3N (0.11 g; 1.1 mmol) were used as reagents for the preparation of $[Fe(AODP)_2](ClO_4)$. Black powder (0.43

g). Yield: 59%. HR-MS (positive mode) m/z calcd. for $[C_{50}H_{34}FeN_{12}S_2]^+$: 922.1815 [M − $ClO_4]^+$. Found: 922.1815. Anal. calcd. $C_{50}H_{34}FeN_{12}S_2 \cdot (ClO_4)$: C, 58.74; H, 3.35; N, 16.44; S, 6.27. Found: C, 58.75; H, 3.51; N, 16.72; S, 6.26.

[Fe(AOAP)$_2$](ClO$_4$)

AOAP (622 mg, 1.67 mmol), $Fe(ClO_4)_3.6H_2O$ (386 mg; 0.84 mmol) and Et_3N (0.11 g; 1.1 mmol) were used as reagents for the preparation of $[Fe(AOAP)_2](ClO_4)$. Brown powder (0.48 g). Yield: 64%. LC-MS (positive mode) m/z calcd. for $[C_{42}H_{32}FeN_{10}S_2]^+$: 796.16 [M – $ClO_4]^+$. Found: 796.10. Anal. calcd. for $[C_{42}H_{32}FeN_{10}S_2] \cdot (ClO_4)$: C, 56.29; H, 3.60; N, 15.63; S, 7.16. Found: C, 56.38; H, 3.23; N, 15.38; S, 7.11.

General synthetic procedure of Cu(II) complexes

NATs (2 mmol) was dissolved in 20 mL of EtOH, and $Cu(ClO_4)_2.6H_2O$ (1 mmol) were added. The mixture was stirred for 20 min at room temperature and then Et_3N (1.1 mmol) was added. The precipitate was filtered off, washed with cold EtOH and Et_2O, and dried *in vacuo*.

[Cu(AOBP)$_2$]

AOBP (510 mg; 1.17 mmol), $Cu(ClO_4)_2.6H_2O$ (217 mg; 0.585 mmol) and Et_3N (0.11 g; 1.1 mmol) were used as reagents for the preparation of $[Cu(AOBP)_2]$. Brown powder (0.12 g). Yield: 23%. LC-MS (positive mode) m/z calcd. for $[C_{52}H_{36}CuN_{10}S_2]$: 928.19 $[M + H]^+$. Found: 928.20. Anal. calcd. for $[C_{52}H_{36}CuN_{10}S_2]$: C, 67.25; H, 3.90; N, 15.02; S, 6.90. Found: C, 67.33; H, 3.83; N, 15.02; S, 6.67.

[Cu(AOAPZ)$_2$]

AOAPZ (622 mg; 1.67 mmol), $Cu(ClO_4)_2 \cdot 6H_2O$ (311 mg; 0.84 mmol) and Et_3N (0.11 g; 1.1 mmol) were used as reagents for the preparation of $[Cu(AOAPZ)_2]$. Brown powder (0.49 g). Yield: 67%. LC-MS (positive mode) m/z calcd. for $[C_{40}H_{30}CuN_{12}S_2]$: 806.15 $[M + H]^+$. Found: 806.30. Anal. calcd. for $[C_{40}H_{30}CuN_{12}S_2]$: C, 59.58; H, 3.75; N, 20.84; S, 7.95. Found: C, 59.39; H, 3.59; N, 20.49; S, 8.13.

[Cu(AOAP)$_2$]

AOAP (598 mg; 1.61 mmol), $Cu(ClO_4)_2 \cdot 6H_2O$ (298; 0.806 mmol) and Et_3N (0.11 g; 1.1 mmol) were used as reagents for the preparation of $[Cu(AOAP)_2]$. Brown powder (0.39 g). Yield: 61%. LC-MS (positive mode) m/z calcd. for $[C_{42}H_{33}CuN_{10}S_2]$: 804.16 $[M + H]^+$. Found: 804.30. Anal. calcd. for $[C_{42}H_{33}CuN_{10}S_2]$: C, 62.71; H, 4.01; N, 17.41; S, 7.97. Found: C, 62.57; H, 4.16; N, 17.72; S, 7.88.

General synthetic procedure of Zn(II) complexes

NATs (2 mmol) was dissolved in 20 mL of EtOH, and $Zn(ClO_4)_2.6H_2O$ (1 mmol) were added. The mixture was stirred for 20 min at room temperature and then Et_3N (1.1 mmol) was added. The precipitate was filtered off, washed with cold EtOH and Et_2O, and dried *in vacuo*.

[Zn(AOBP)$_2$]

AOBP (658 mg; 1.52 mmol), $Zn(ClO_4)_2.6H_2O$ (283 mg; 0.76 mmol) and Et_3N (0.11 g; 1.1 mmol) were used as reagents for the preparation of $[Zn(AOBP)_2]$. Orange powder (0.35 g). Yield: 49%. LC-MS (positive mode) m/z calcd. for $[C_{52}H_{36}N_{10}S_2Zn]$: 929.19 $[M + H]^+$. Found: 929.30. ^{1}H NMR (800 MHz, d_6-DMSO) δ 11.20, 10.30 (s, 1H), 8.47 (d, J = 44.7 Hz, 1H), 8.28 – 8.11 (m, 4H), 8.03 – 7.85 (m, 2H), 7.74 – 7.55 (m, 3H), 7.53 – 7.36 (m, 3H), 7.29 – 7.15 (m,

2H), 7.10 – 6.86 (m, 2H). ^{13}C NMR (201 MHz, d_6-DMSO) δ 191.13, 151.35, 149.87, 149.52, 146.97, 143.89, 140.28, 139.95, 133.99, 132.54, 132.39, 130.51, 129.97, 129.73, 129.62, 129.39, 128.99, 128.84, 127.85, 125.87, 125.63, 125.36, 124.71, 124.33, 123.53, 117.03. Anal. calcd. for [$C_{52}H_{36}N_{10}S_2Zn$]: C, 67.12; H, 3.90; N, 15.05; S, 6.89. Found: C, 67.39; H, 3.80; N, 15.06; S, 6.53.

[Zn(AOAPZ)$_2$]

AOAPZ (622 mg; 1.67 mmol), $Zn(ClO_4)_2.6H_2O$ (313 mg; 0.84 mmol) and Et_3N (0.11 g; 1.1 mmol) were used as reagents for the preparation of [$Zn(AOAPZ)_2$]. The compound was then recrystallized in MeOH, and a mixture of EtOH: DCM 50:50 (*v/v*) used for crystal growth. Red powder (0.45 g). Yield: 67%. LC-MS (positive mode) m/z calcd. for [$C_{40}H_{30}N_{12}S_2Zn$]: 807.15 $[M + H]^+$. Found: 806.95. ^{1}H NMR (800 MHz, d_6-DMSO) δ 11.26, 10.36 (s, 1H), 9.32 (d, J = 21.1 Hz, 1H), 9.12 (d, J = 17.5 Hz, 1H), 8.93 – 8.80 (m, 1H), 8.23 (d, J = 47.4 Hz, 3H), 8.07 – 7.84 (m, 1H), 7.68 – 7.52 (m, 2H), 7.41 (d, J = 8.0 Hz, 1H), 7.01 (s, 1H), 2.75 (d, J = 24.0 Hz, 3H). ^{13}C NMR (201 MHz, d_6-DMSO) δ 189.81, 149.83, 149.54, 148.14, 146.96, 146.57, 144.95, 144.65, 140.98, 140.67, 140.31, 132.49, 130.69, 129.54, 128.82, 125.70, 123.77, 120.99, 117.28, 14.49-13.72. Anal. calcd. for [$C_{40}H_{30}N_{12}S_2Zn$]: C, 59.44; H, 3.74; N, 20.79; S, 7.93. Found: C, 59.39; H, 3.80; N, 20.66; S, 7.71.

X-ray crystallographic studies

Crystallographic data were collected on an Oxford Diffraction Gemini Ultra S diffractometer with Cu Kα radiation (1.54184 Å) at 190 K. Structures were solved using SHELXT, and refinement performed with SHELXL.[11] Mercury (CCDC) was used for generating all diagrams of the structures, with the crystallographic data in CIF format being deposited with the CCDC. The CCDC numbers are presented below in **Table S1**.

Biological Studies

Cell culture

Human DMS-53 small cell lung carcinoma cells, HCT-15 colorectal adenocarcinoma cells, and KB31 (Pgp-) and KBV1 (Pgp+) cervical carcinoma cells were purchased from the American Type Culture Collection (ATCC®, Manassas, VA). The DMS-53 and HCT-15 cells were grown in RPMI 1640 (Invitrogen, Carlsbad, CA) media. KBV1 (Pgp+), and KB31 (Pgp-) cells were grown in DMEM media.

All media were supplemented with 10% fetal bovine serum (10%), non-essential amino acids (1 mM), sodium pyruvate (1 mM), and L-glutamine/penicillin-streptomycin (1 mM). The cells were grown using standard techniques in an incubator (Forma Scientific, Marietta, OH, USA) at 37 ºC within a humidified atmosphere containing 95% air/5% CO_2.[3, 12, 13] The provider assessed the authenticity of cells through viability, recovery, growth, and morphology, as well as cytogenetic analysis, antigen expression, DNA profiling, and isoenzyme analysis. Mycoplasma contamination in the cells was regularly monitored by standard procedures.[14]

Cellular proliferation assay

Proliferation was assessed using the well-established 3-(4, 5-dimethylthiazol-2-yl)-2,5-diphenyltetrazolium bromide (MTT) based cell viability assay.[15-18] The formation of formazan product correlated directly with cellular viability as determined by Trypan blue staining.[12] The compounds were dissolved in DMSO to prepare a stock solution of 10 mM on the day of the study and then immediately diluted in culture media without storage.

For the culture experiments, the maximum concentration of DMSO did not exceed 0.5% (v/v). Cells were seeded in 96-well plates (6,000-15,000 cells/well) and were incubated with serial

dilutions of the compounds for 24, 48, or 72 h/37 °C. After the treatments, thiazolyl blue tetrazolium bromide (MTT) in PBS (5 mg/mL) was added to the plate and incubated for an additional 2 h/37 °C. The media was then aspirated, and 100 µL of DMSO was added to each well to solubilize the cells, followed by 5 min of shaking the plates. Absorbance of MTT was measured using a CLARIOstar microplate reader (at 570 nm). Data analysis was performed using MARS Data Analysis Software (BMG LabTech, version 3.30), subsequently determining the concentration of agents inhibiting proliferation by 50% (*i.e.*, IC_{50}).

In studies examining the effect of Elacridar (Ela), KBV1 (+Pgp), KB31 (-Pgp), DMS-53, and HCT-15 cells were pre-incubated in the presence or absence of Ela (0.2 µM) for 1 h/37 °C prior to treatment for 24 h/37 °C with the ligands or their complexes (0.012-25 µM) in the presence and absence of Ela (0.2 µM). The IC_{50} values were then calculated.

Genetic silencing of Pgp via small interfering RNA (siRNA)

A non-targeting negative control siRNA (siControl; Cat.#: 4390843, Thermo Fisher Scientific), and siRNA specific for *Pgp* (siPgp; Cat.#: AM51333; Invitrogen, Carlsbad, CA) were used. Sequences of each siRNA are available online from the suppliers. The siRNAs were reverse transiently transfected into KBV1 (+Pgp), KB31 (-Pgp), DMS-53, and HCT-15 cells using Lipofectamine RNAiMAXR (Cat.#: 13778100; Invitrogen), and incubated for 72 h/37°C. Then total cellular protein extraction and western blotting was performed, as described below.

Protein extraction from cells, SDS-PAGE, and western blot analysis

Established methods were used for protein extraction, SDS-PAGE and Western blot analysis.[19, 20] Cells from the culture substratum using 1 mM EDTA in Ca^{+2}/Mg^{+2}-free PBS, with the cell suspensions being disrupted on ice using a sonicator (Branson, MO), followed by

centrifugation at 13,200 rpm/40 min/4°C. The supernatant was then separated from the pellet and the protein concentration examined by implementing the bicinchoninic acid (BCA) protein assay kit (Thermo Fisher Scientific) and a UV-Vis spectrophotometer (Shimadzu, Kyoto, Japan).

Lysates were prepared from cells after the addition of β-mercaptoethanol (Sigma-Aldrich) and then heated for 5 min/95°C. SDS-PAGE (8, 10, or 12% gels) was then performed, with the proteins being transferred for 24 h onto a PVDF membrane (0.45 μM pore size; Millipore, MA) at 30 V/4°C. After the transfer, the membrane was soaked in 100% methanol for 30 s and dried at 37°C/2 h.

Membranes were subsequently blocked using 5% skim milk and/or bovine serum albumin (BSA; Cat.#:A9418 Sigma-Aldrich) solution in TBS-T for 1.5 h/20°C. Primary antibodies were diluted in 5% skim milk or BSA in TBS-T and incubated with the membranes for 24 h/4°C. The membranes were then incubated with secondary antibody diluted in 5% skim milk for 1 h/20°C, followed by washing in TBS-T (3 times/5 min//20°C). The primary and secondary antibody was against Pgp (Abcam; Cat.#: ab170904), while the secondary antibody was from Sigma (Cat.#: A1654). The specificity of each antibody was validated by the suppliers and supported by the assessment of the molecular weight of each protein detected (*via* molecular weight markers).

The antibody-antigen complex was detected after incubation with Western HRP substrate (Cat no. WBLUF0500: Millipore) for 1 min. The signal generated was imaged with a Sapphire Biomolecular Imager (Azure Biosystems, CA). Signals were normalized to the protein loaded

to each lane (80 μg/lane), with equal loading being examined relative to the house keeping protein, β-actin.

Examining thiosemicarbazone nuclear localization with confocal microscopy

This nuclear localization study is important as it provides insights into the intricate mechanisms involved in the newly synthesized NATs, which were assessed using HCS NuclearMask™ Deep Red (Cat. #H10294; Invitrogen™). The KBV1 (Pgp+) and KB31 (Pgp-) cells were treated with 60 nM of NuclearMask™ Deep Red for 30 min/37 °C, before the addition of [$Zn(DpC)_2$], AOBP, or AOAP (25 μM), and the cells then incubated for 2 h/37 °C.

Cells were subsequently washed 3 times with HBSS prior to imaging in Live Cell Imaging Solution (Invitrogen™). Excitation wavelengths were set at 405 and 638 nm, and emission detected between 410-500 nm and 685−695 nm. Images were acquired using an Olympus FV3000RS NIR laser scanning confocal microscope with a 40× air objective. Data analysis was performed using ImageJ v1.48 software and Pearson's correlation coefficient was determined using the associated JACoP plugin.[21]

Examination of thiosemicarbazone lysosomal localization using confocal microscopy

The intracellular localization of inherently fluorescent AOBP and AOAP was examined relative to [$Zn(DpC)_2$] that is known to accumulate in lysosomes.[22] To examine co-localization between the lysosomal-specific fluorescent probe, LysoTracker™ Deep Red (Cat. #L12492, Invitrogen™) and AOBP, AOAP, or [$Zn(DpC)_2$], KBV1 (Pgp+) and KB31 (Pgp-) cells were incubated with the agents for 2 h/37ºC. Following this incubation, the cells were washed three times with HBSS at room temperature.

For live cell imaging, the cells were incubated with LysoTracker™ Deep Red (Lysotracker™) for 30 min/37ºC and then imaged in fresh HBSS. The excitation wavelength was set at 405 nm and 647 nm for the drug treatments and LysoTracker™ red, respectively. Emission was detected between 410-500 nm and 668 nm for the drug treatments, and LysoTracker™ red, respectively. Images were acquired using an Olympus FV3000RS NIR laser scanning confocal microscope with a 40× air objective. Data analysis was performed using ImageJ v1.48 software and Pearson's correlation coefficient was determined using the associated JACoP plugin.[21]

Statistics

All experiments were repeated at least three times. The data exhibited a normal distribution around the mean and were analyzed using Student's paired *t*-test. Results are presented as mean ± standard deviation (SD) and were considered statistically significant when $p < 0.05$.

Table S1. Crystal and refinement data.

	AOBP	**AODP.MeCN**	**AOAPZ**	**$[Zn(AOAPZ)_2].CH_3OH.C_2H_5OH$**	**$[AOBP\text{-}S](ClO_4)\cdot CH_2Cl_2$**
Formula	$C_{26}H_{19}N_5S$	$C_{27}H_{21}N_7S$	$C_{20}H_{16}N_6S$	$C_{43}H_{40}N_{12}O_2S_2Zn$	$C_{27}H_{20}Cl_3N_5O_4$
M.W.	433.52	475.57	372.45	836.36	584.83
Crystal system	Monoclinic	Triclinic	Triclinic	Triclinic	Triclinic
Space group	$P2_1/n$	$P\bar{1}$	$P\bar{1}$	$P\bar{1}$	$P\bar{1}$
a (Å)	13.027(1)	7.5694(5)	8.8060(5)	12.7994(5)	7.6716(4)
b (Å)	12.4547(8)	8.9780(7)	9.4077(5)	13.0450(5)	11.4509(7)
c, (Å)	14.718(1)	18.756(1)	11.8916(6)	13.6798(6)	15.546(1)
α (°)		83.796(6)	109.261(5)	100.070(2)	102.548(5)
β (°)	114.83(1)	89.902(6)	101.174(4)	99.897(2)	98.148(4)
γ (°)		65.641(7)	65.641(7)	103.258(2)	103.294(5)
V (Å)^3	2167.2(4)	1153.1(2)	872.43(9)	2134.8(2)	1270.6(1)
T (K)	190(2)	190(2)	190(2)	150(2)	190(2)
Z	4	2	2	2	2
R_1 (obs. data)	0.0477	0.0464	0.0446	0.0462	0.0566
wR_2 (all data)	0.1086	0.1113	0.1244	0.1289	0.1444
GOF	1.020	1.037	1.048	1.048	1.054
CCDC	2355274	2355275	2355276	2359500	2355277

Table S2: The quantum yield (Φ) values of *N*-acridine thiosemicarbazones (NATs) and their Fe(III), Cu(II) and Zn(II) complexes. The quantum yield was estimated using acridine orange (φ = 0.20) as a reference.[23]

Compound	$\Phi \times 10^{-3}$
AOBP	0.69
$[Fe(AOBP)_2]^+$	0.79
$[Cu(AOBP)_2]$	0.36
$[Zn(AOBP)_2]$	0.76
AODP	0.15
$[Fe(AODP)_2]^+$	0.74
AOAPZ	0.76
$[Cu(AOAPZ)_2]$	0.82
$[Zn(AOAPZ)_2]$	0.81
AOAP	0.88
$[Fe(AOAP)_2]^+$	0.92
$[Cu(AOAP)_2]$	0.79

Supplementary Results and Discussion

X-ray Crystallography

Precise elucidation of the structure of the ligands and complexes by X-ray crystallography helps to dissect structure-activity relationships and understand biological activity. The structures of AOBP (**Figure S1A**), AODP (**Figure S1B**), and AOAPZ (**Figure S1C**) were determined and the crystal refinement parameters presented in **Table S1**, with the ligand packing diagrams shown in **Figure S2A-C**. For the thiosemicarbazone ligands from this family, *N1*, *N2* and *S1* are the donor atoms that will coordinate to metal ions in a meridional fashion (**Figure S1A-C**).

It is notable that the N1-diaryl ligands, AOBP and AODP, are in the *Z*-isomeric conformation, while the electron-rich monoaryl ligand, AOAPZ, is an *E*-isomer (**Figure S1A-C**). In all cases, metal ion coordination will require significant conformational rearrangement of the ligands. The molecular structure of AOBP features an intramolecular hydrogen bond (**Figure S1A**) (N3−H3A…N1 1.97 Å, 133.4°) facilitated by the *Z*-isomeric conformation of the pyridine-imine group. Packing is stabilized by π-π and π-edge interactions. Notably, the acridine moiety participates in a classic slipped π-π interaction with a symmetry-related molecule being evident (symmetry code -x, 1-y, 1-z; **Figure S1A**). The pyridine and benzene moieties both have larger numbers of longer-range, and thus, weaker π-edge interactions.

The structure of AODP·MeCN reveals a different tautomeric form with the proton formerly on N4 moving to N6 on the acridine group (**Figure S1B**). This is associated with markedly shorter N4–C13 and N4-C12 bonds (~1.31 Å), while the thione C12=S1 bond is lengthened. The bonding is best described by the resonance structures shown in **Figure S3A**, one in the zwitterionic state and the other being neutral. Intramolecular H-bonding with the pyridyl N1

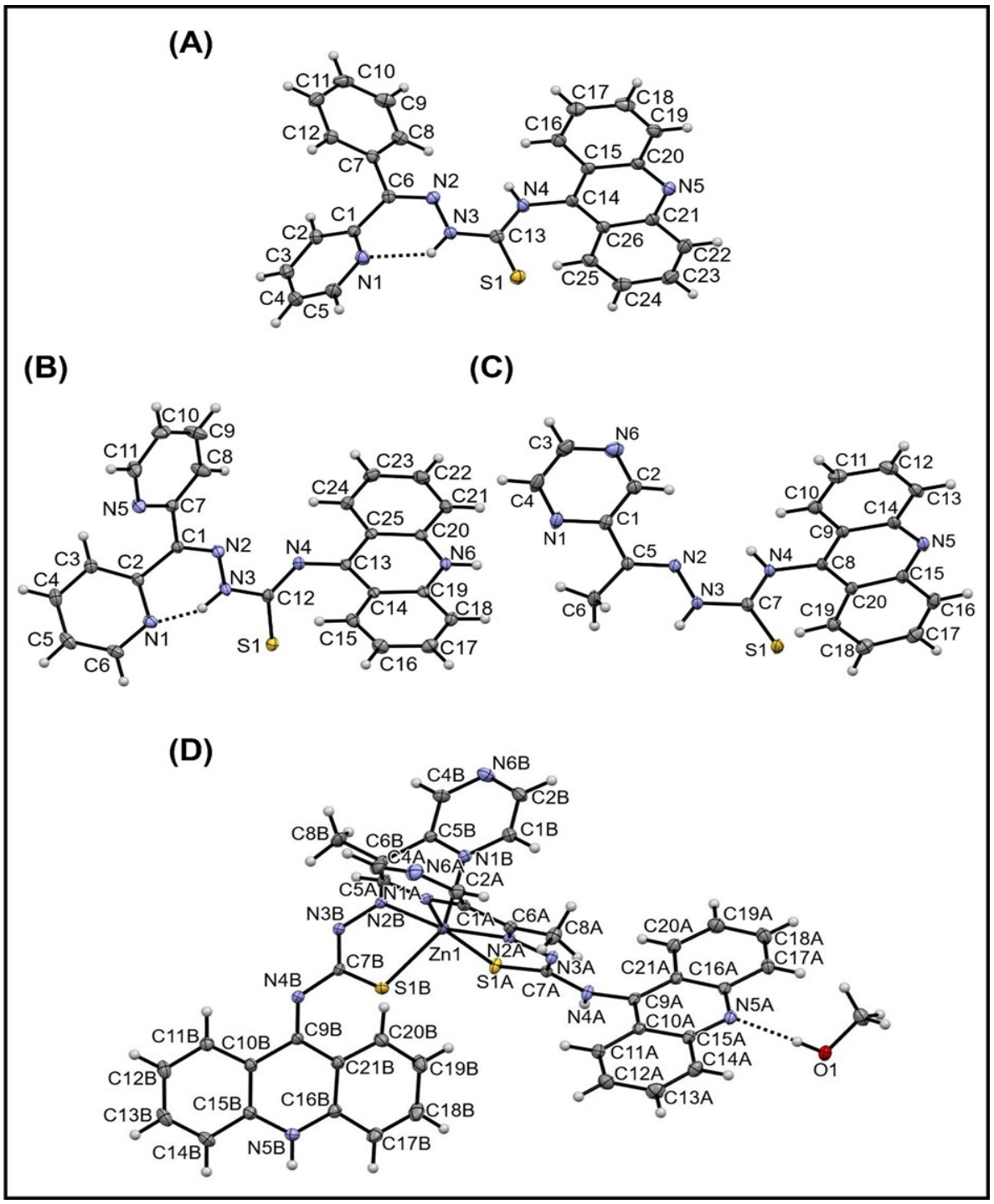

Figure S1A-D. ORTEP views (30% ellipsoids) and selected bond lengths (Å) of: **(A)** AOBP: C13−S1 1.668(2), C13−N3 1.354(2), C13−N4 1.343(3), C14−N4 1.427(2); **(B)** AODP·MeCN (MeCN not shown): C12−S1 1.703(2), C12−N3 1.370(2), C12−N4 1.316(3), C13−N4 1.315(2); **(C)** AOAPZ: C7−S1 1.667(2), C7−N3 1.365(2), C7−N4 1.340(2), C8−N4 1.429(2), and **(D)** $[Zn(AOAPZ)_2]$·MeOH·EtOH (EtOH not shown): N(1A)-Zn(1) 2.249(2), N(1B)-Zn(1) 2.266(2), N(2A)-Zn(1) 2.131(2), N(2B)-N(3B) 1.380(3), N(2B)-Zn(1) 2.124(2), S(1A)-Zn(1) 2.4238(8), S(1B)-Zn(1) 2.4191(8) Å.

atom and thiosemicarbazone N3-H group being again a feature. The structure of AOAPZ (**Figure S1C**) reveals the same tautomeric form as AOBP (**Figure S1A**). The most significant difference is the *E*-conformation of the pyrazine-imine group, which prevents intramolecular H-bonding. Instead, centrosymmetric H-bonded dimers form that involve the thiosemicarbazone NH and the S-atom (N3-H3A… S1′ 2.62 Å, 169.6° symmetry operation −x, −y+1, −z; **Figure S1C**).

The preparation of the AOAPZ Fe(III) complex led to an unstable product, as the complexation reaction often resulted in desulfurization and cyclization of the ligand. A similar product was observed during the crystallization of $[Fe(AOBP)_2]^+$, leading to an unusual bicyclic structure in the form of its perchlorate salt, where H_2S was eliminated from the thiosemicarbazone (**Figure S3B, C**). The precise mechanistic details of this conversion are not yet understood and were not the focus of this investigation.

In contrast to the Fe(III) complex, preparation of $[Zn(AOAPZ)_2]\cdot MeOH\cdot EtOH$ resulted in the typical 2:1 ligand (L): Zn(II) complex, revealing an expected distorted octahedral geometry, with both ligands binding in a meridional conformation (**Figure S1D**). Deprotonation of both AOAPZ ligands at N3A/B results in a significant reduction in the C7A/B═N3A/B bond lengths (average 1.321(4) Å) and an increase in the C7A/B–S1A/B bond length (average 1.731(3) Å) relative to the free ligand (**Figure S1C**).[2, 24] This structural feature corresponds to the predominant iminethiolate resonance form (N═C–S^-), rather than the thioamide [(H)N–C═S], which aligns more closely with neutral free ligand.[24] Several similar 1:2 Zn(II)−thiosemicarbazone complexes have been reported previously.[2, 24-28]

In the crystal structure of $[Zn(AOAPZ)_2]\cdot MeOH\cdot EtOH$, one methanol molecule forms a hydrogen bond with an acridine nitrogen atom (N5A; **Figure S1D**), stabilizing the molecular packing (**Figure S2D**). The two acridine groups exist in different tautomeric forms, with a proton located on N4A and N5B. With protonation of N4A, the N4A-C9A bond is formally a single bond (length: 1.416 Å). Conversely, with the proton on N5B, the N4B-C9B bond is a double bond (length: 1.299 Å). These differences mirror the bond length changes observed in the different free ligand tautomers in **Figure S1B** (acridine ring N6 protonated) and **Figures S1A** and **S1C** (N4 protonated). The various tautomeric forms of $[Zn(AOAPZ)_2]$ and its potential hydrogen bonding interactions could influence its interactions with biological molecules, and thus, its activity.

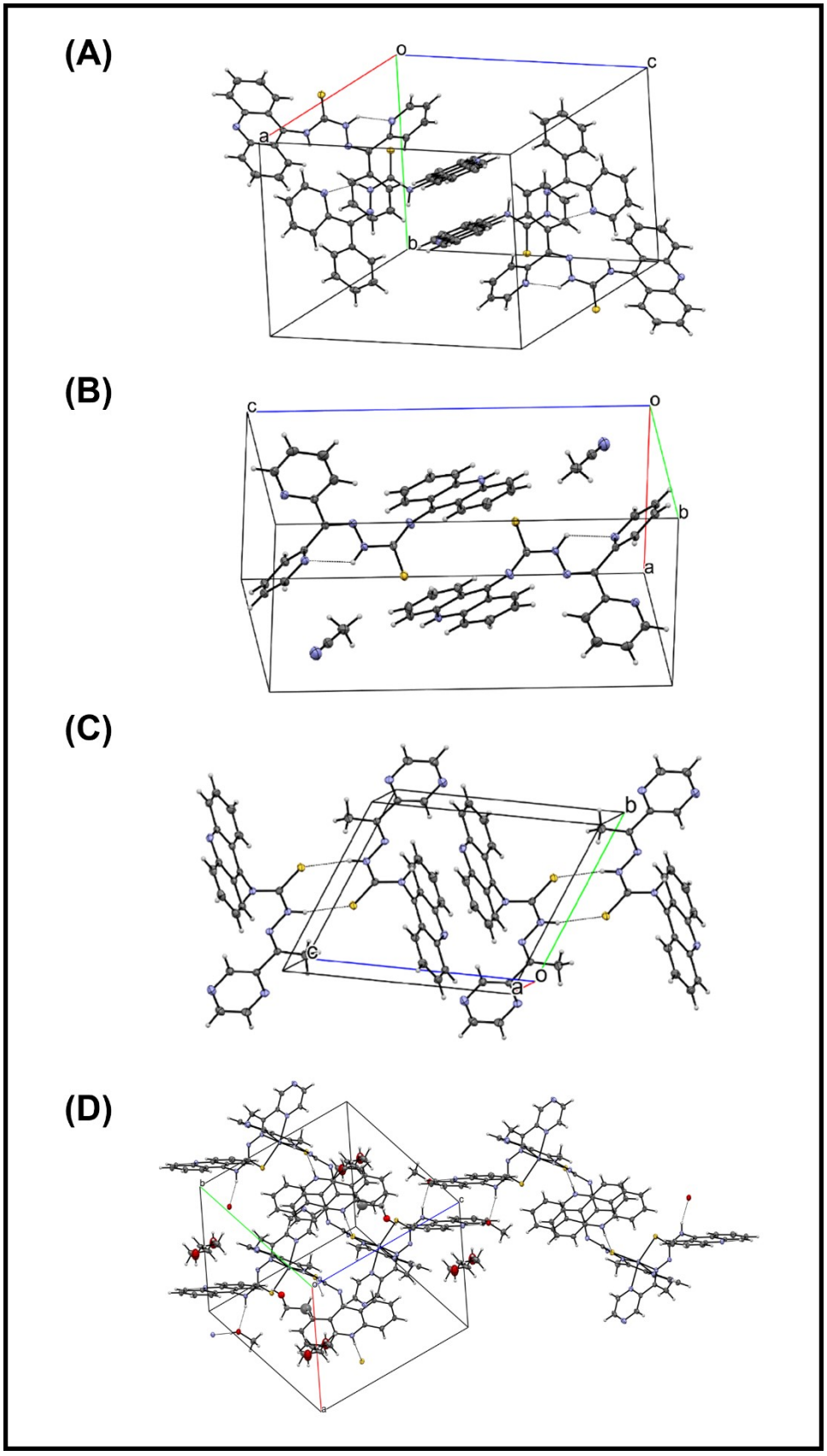

Figure S2: Crystal packing diagrams for **(A)** AOBP, **(B)** AODP·MeCN, **(C)** AOAPZ, and **(D)** [Zn(AOAPZ)$_2$].

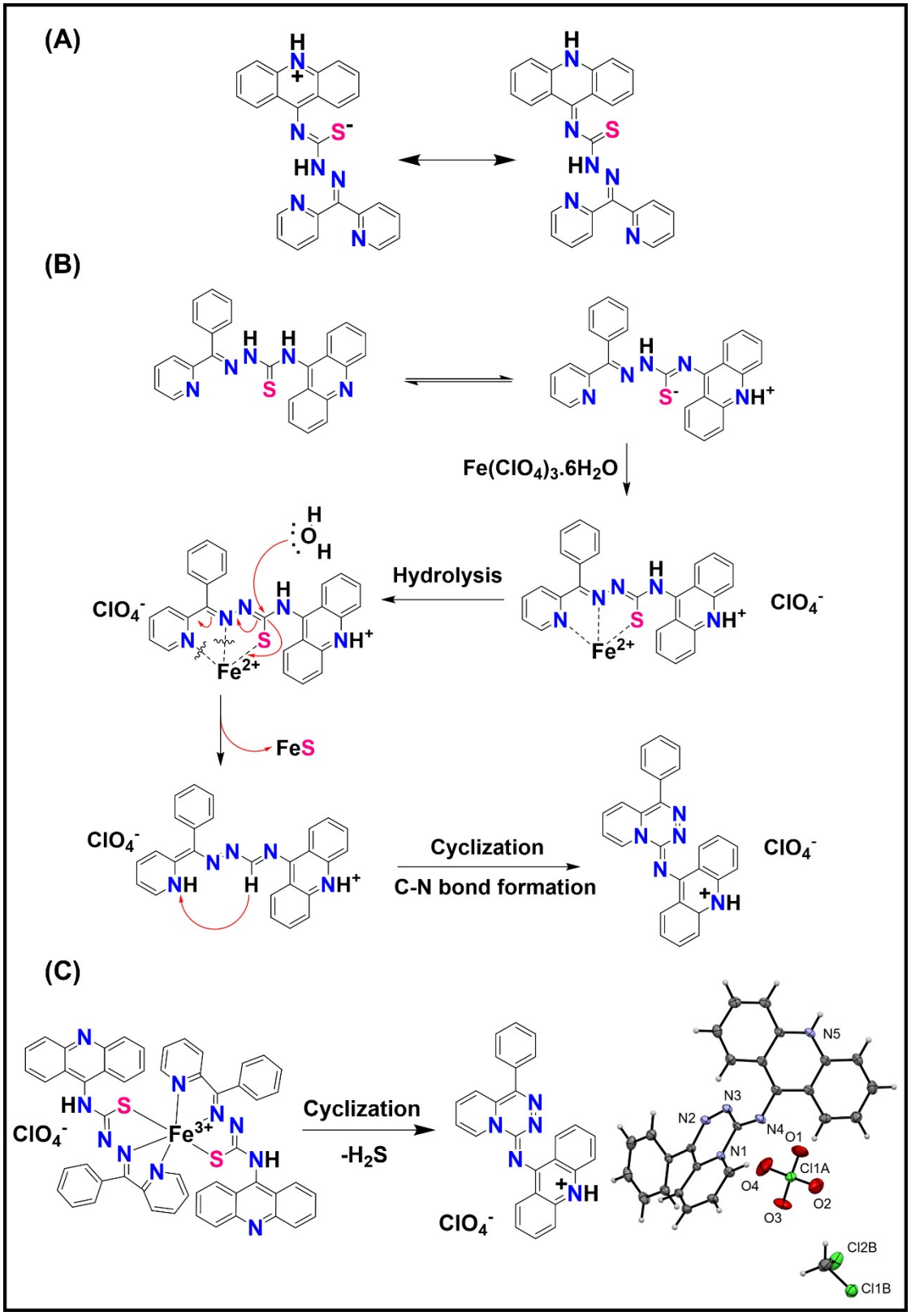

Figure S3: **(A)** Two of the relevant resonance structures of AODP. **(B)** Speculated mechanism of desulfuration and cyclisation of the Fe(AOBP) complex based on references[29, 30]; (**C**) Desulfuration and cyclization of $[Fe(AOBP)_2]^+$ during crystallization and crystal structure of $(AOBP\text{-}S)(ClO_4).CH_2Cl_2$ (30% ellipsoids). This mechanism of desulfuration and cyclization was not a focus of the current investigation, with the precise details not being experimentally examined.

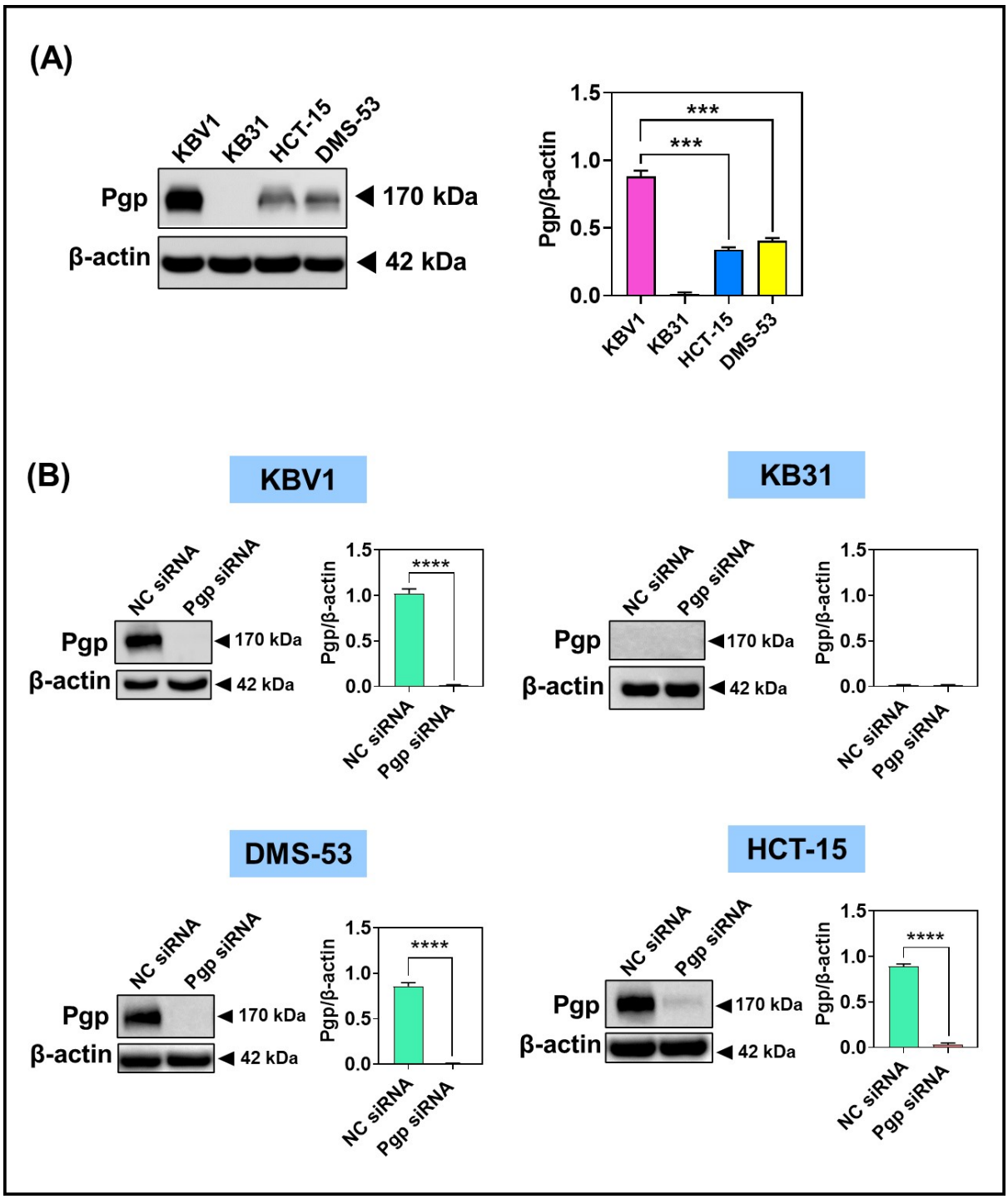

Figure S4. (A) Western blot demonstrating the relative levels of Pgp in KBV1 (+Pgp) cells, KB31 (-Pgp) cells, DMS-53 small cell lung carcinoma cells, and HCT-15 colon adenocarcinoma cells. **(B)** Western blot demonstrating the down-regulation of Pgp protein levels in each of the cell-types in **(A)** after incubation with Pgp siRNA for 72 h/37°C *versus* the non-targeting negative control (NC) siRNA. Densitometric analysis is relative to the β-actin protein loading control. Western blots are from a typical experiment, while the densitometry is the mean ± S.D. of three experiments, ***p *versus* KBV1 (+ Pgp) cells and ****$p < 0.0001$ *versus* the NC siRNA, respectively.

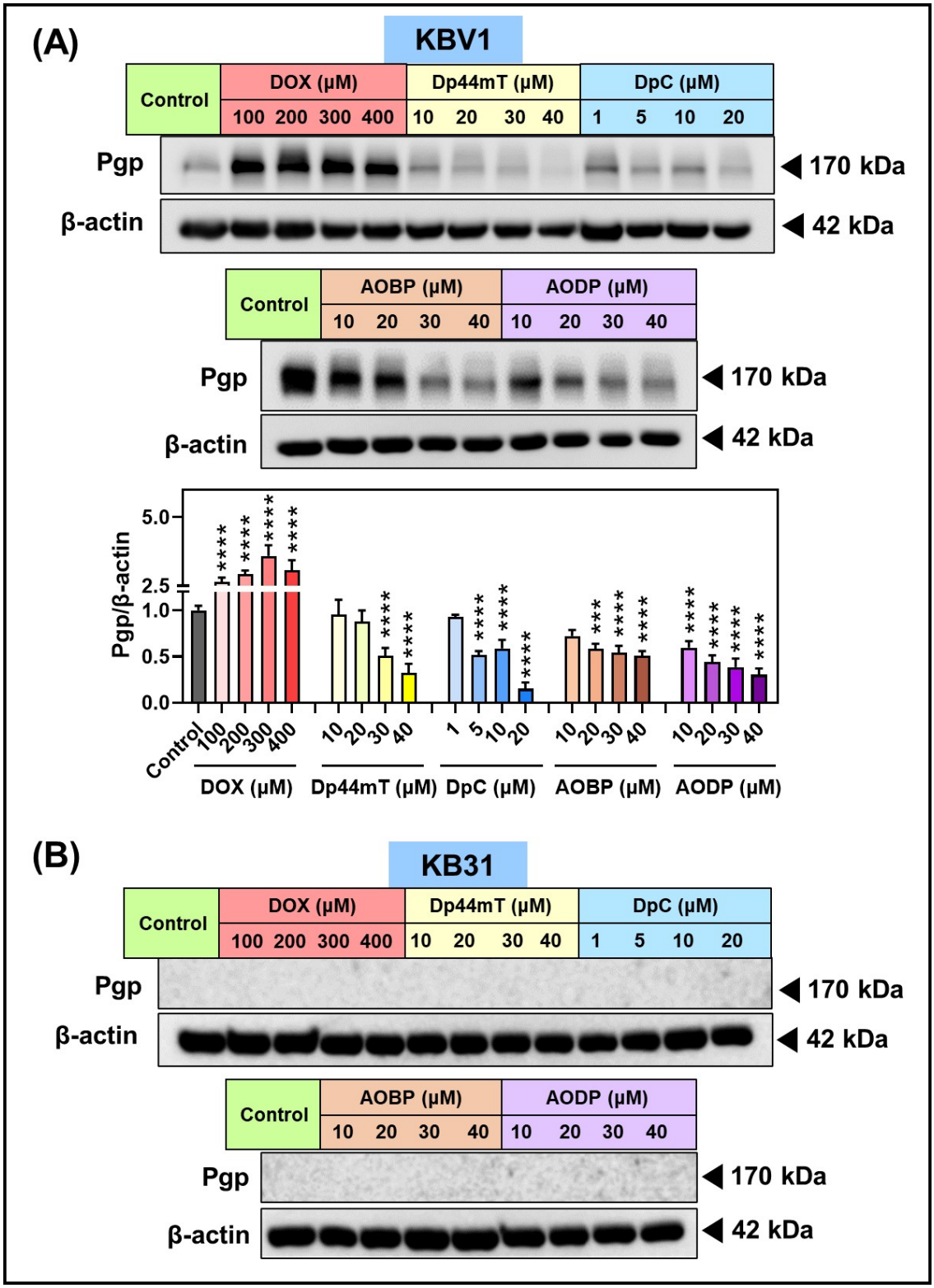

Figure S5. Pgp protein expression in KBV1 (+Pgp) cells is increased by DOX, but decreased by Dp44mT, DpC, AOBP, or AODP. **(A)** Western blot analysis of Pgp expression in KBV1 cells (+Pgp) after a 48 h/37 °C incubation with DOX (100-400 μM), Dp44mT (10-40 μM), DpC (1-20 μM), AOBP (10-40 μM), AODP (10-40 μM) *versus* control media alone. **(B)** Western blot analysis of Pgp expression in KB31 (-Pgp) cells under the same conditions as in **(A)**, as a negative control. Western blots are from a typical experiment while the densitometry is the mean ± S.D. of three experiments, ***, $p < 0.001$; ****, $p < 0.0001$ *versus* the control.

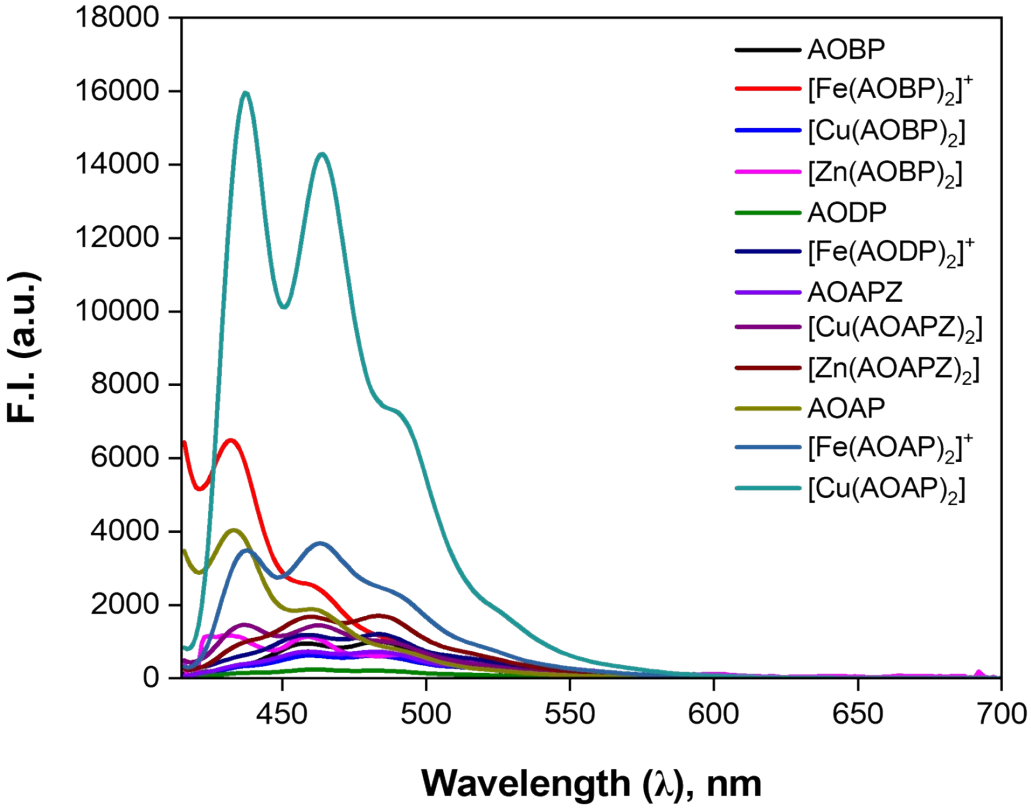

Figure S6. Fluorescence spectra of AOBP, $[Fe(AOBP)_2]^+$, $[Cu(AOBP)_2]$, $[Zn(AOBP)_2]$, AODP, $[Fe(AODP)_2]^+$, AOAPZ, $[Cu(AOAPZ)_2]$, $[Zn(AOAPZ)_2]$, AOAP, $[Fe(AOAP)_2]^+$, and $[Cu(AOAP)_2]$ measured in DMSO following excitation at 400 nm.

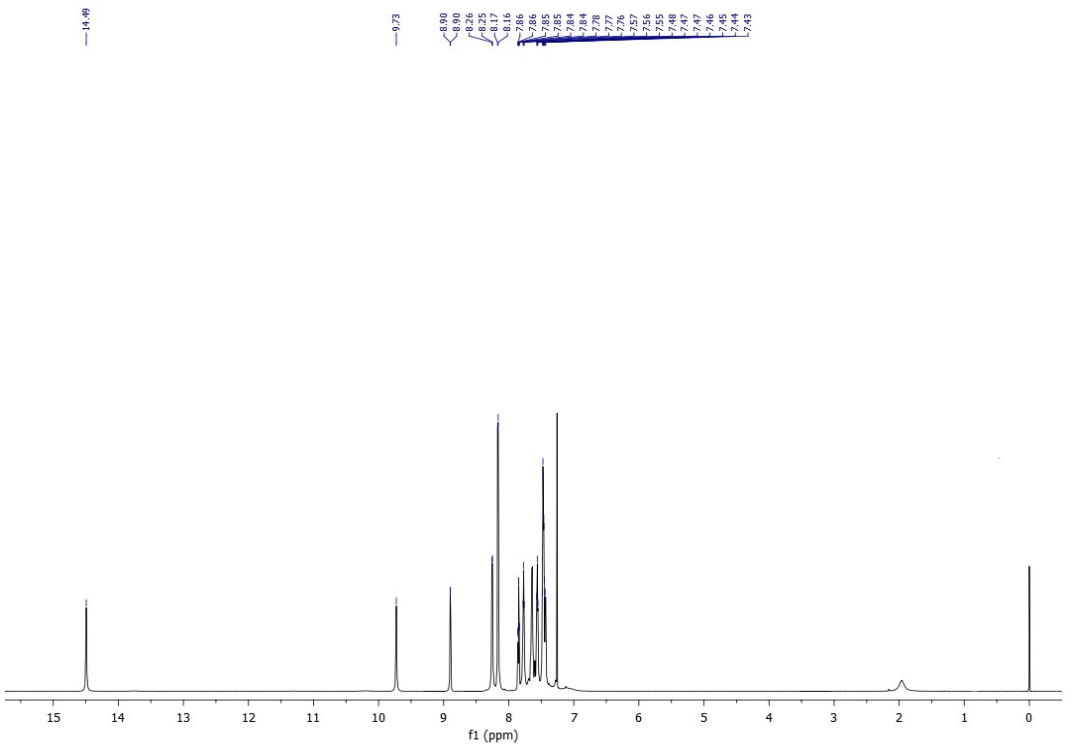

Figure S7. ^{1}H NMR spectrum of AOBP.

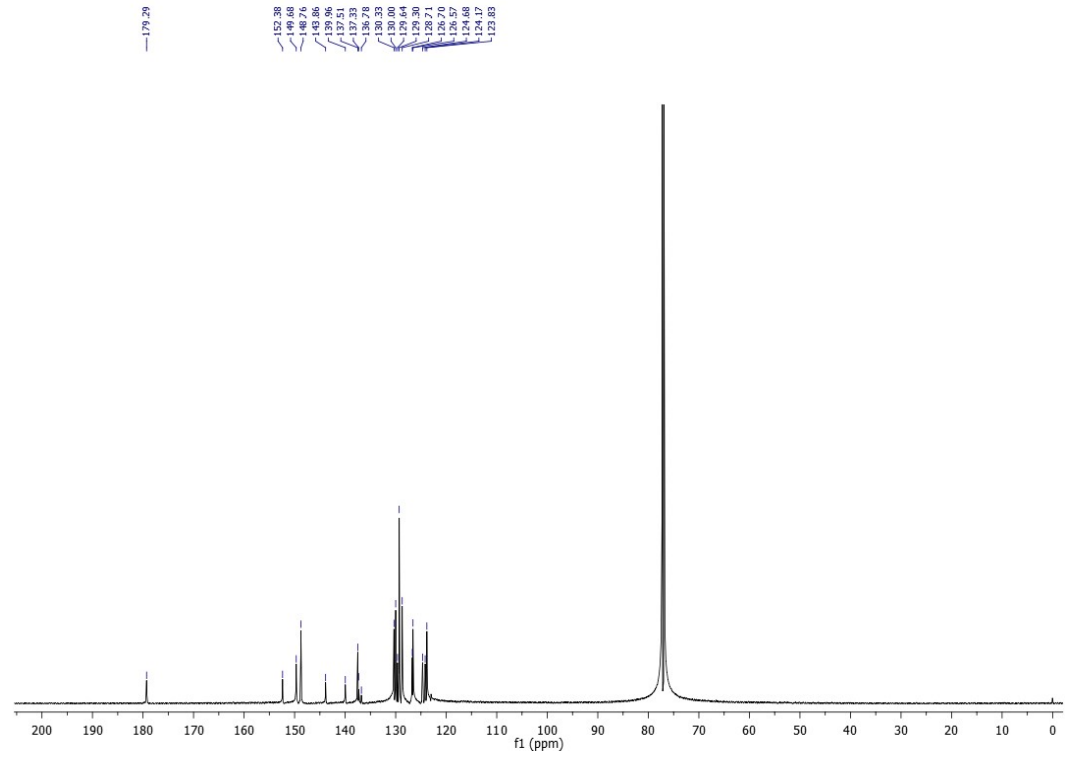

Figure S8. ^{13}C NMR spectrum of AOBP.

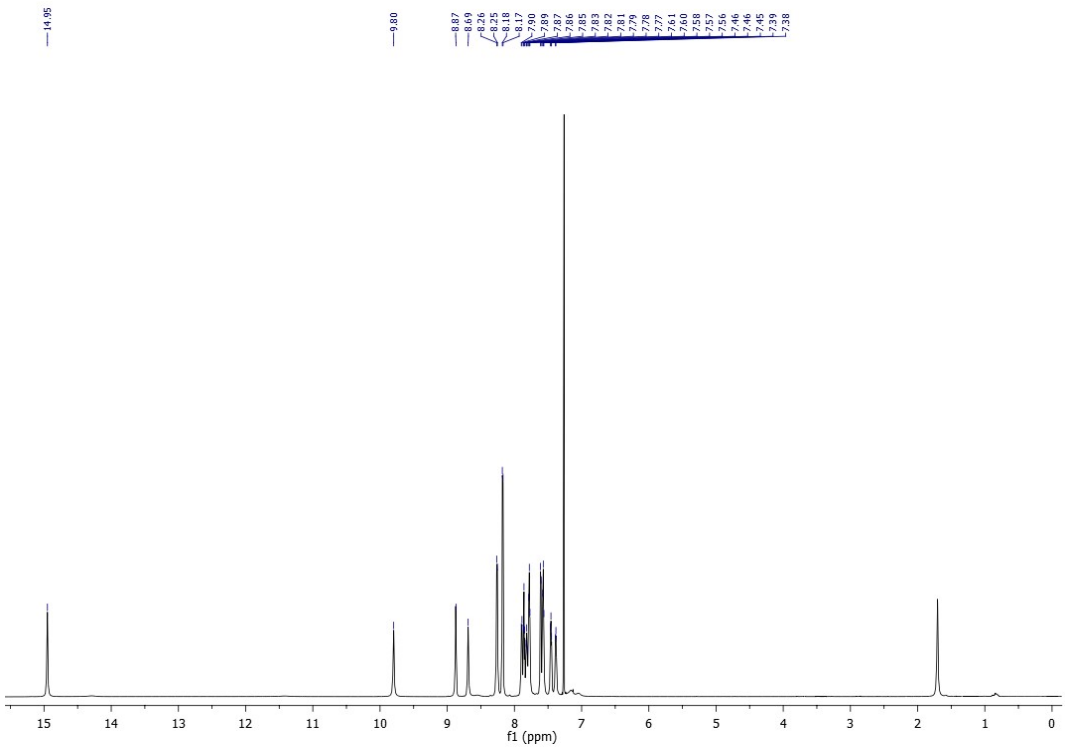

Figure S9. ^{1}H NMR spectrum of AODP.

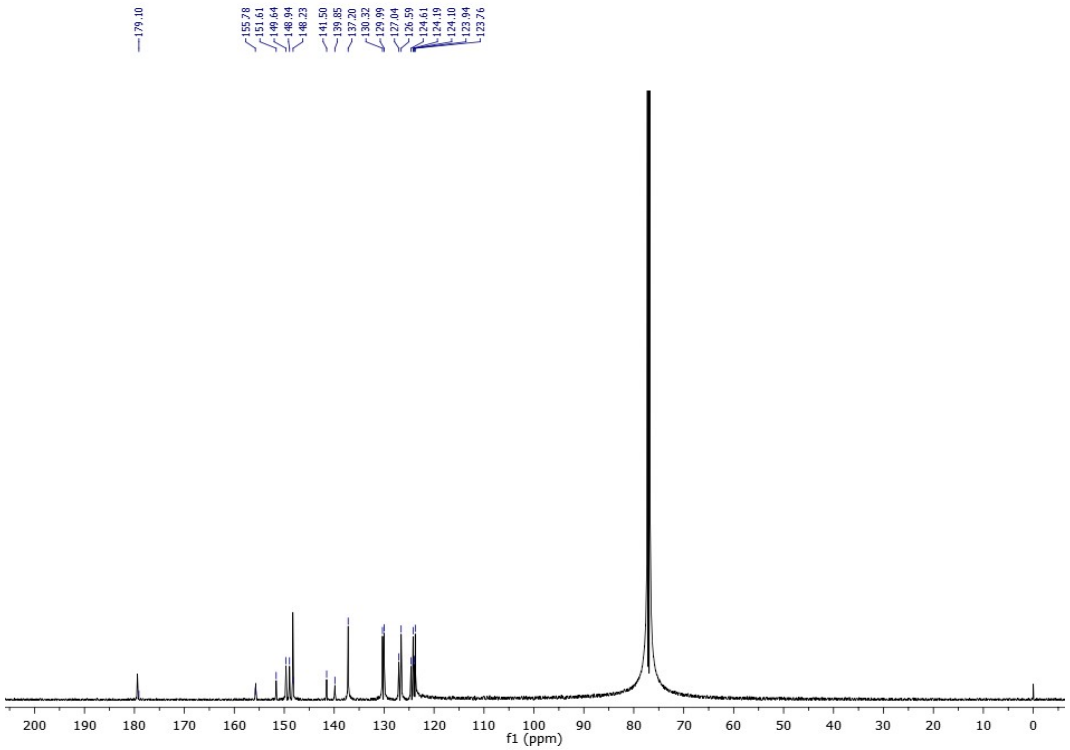

Figure S10. ^{13}C NMR spectrum of AODP.

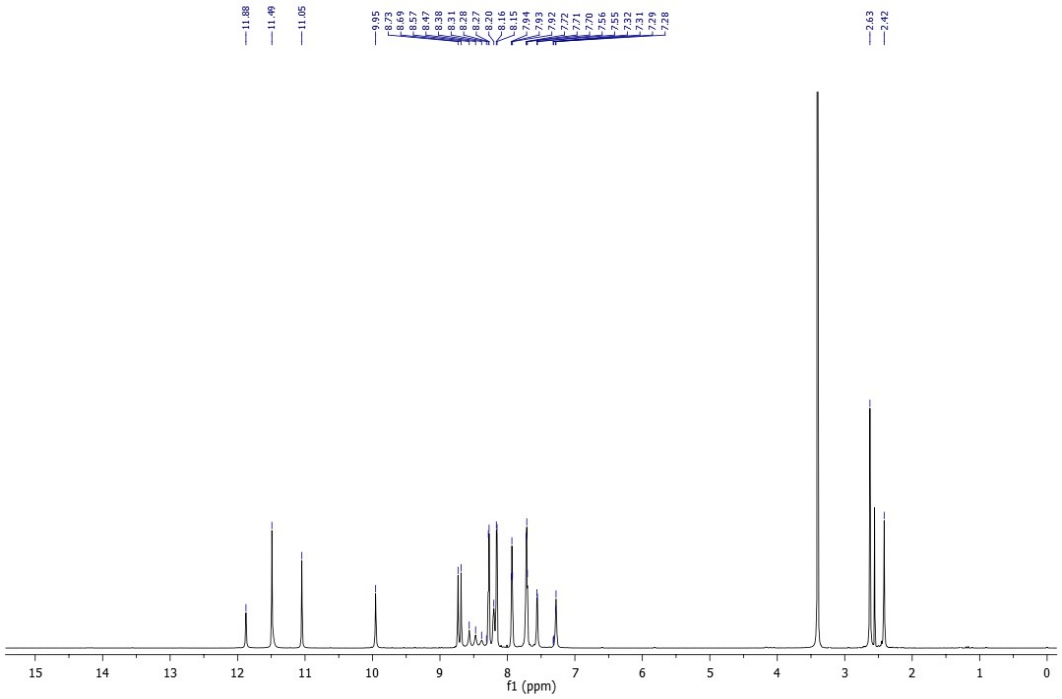

Figure S11. ^{1}H NMR spectrum of AOAPZ.

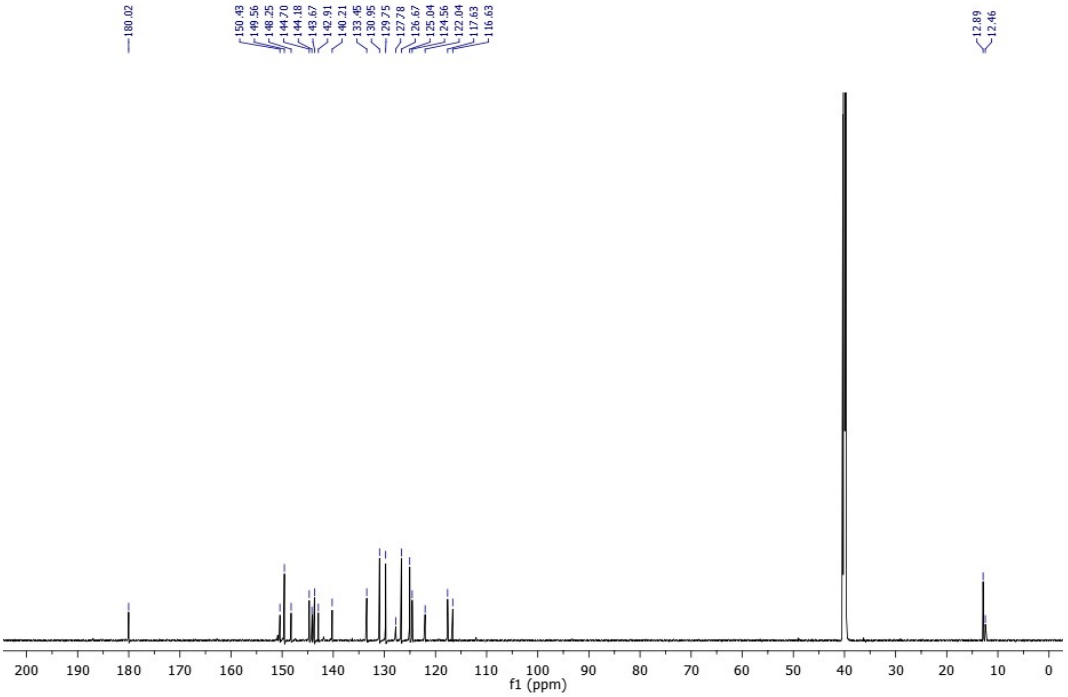

Figure S12. ^{13}C NMR spectrum of AOAPZ.

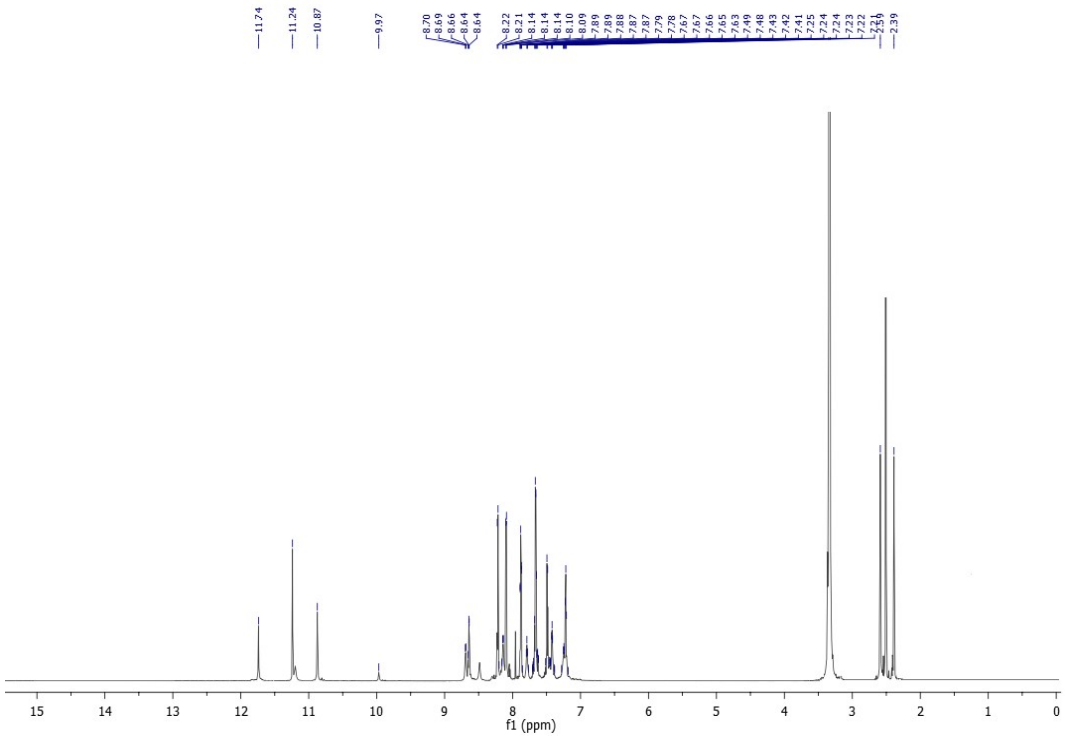

Figure S13. ^{1}H NMR spectrum of AOAP.

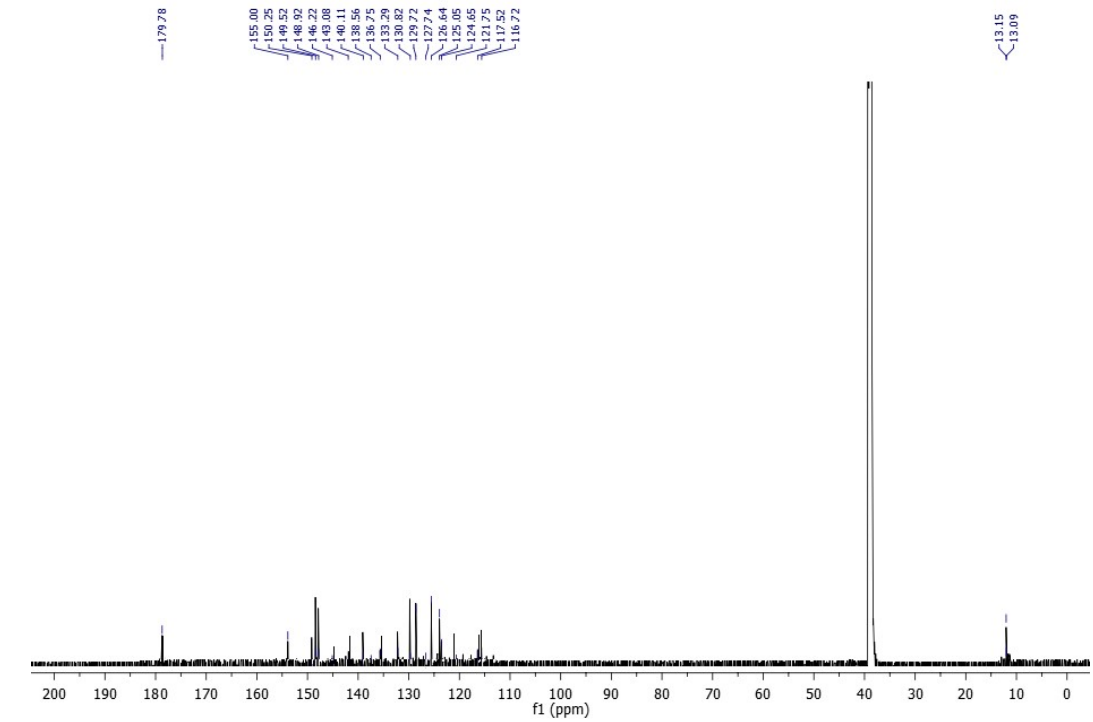

Figure S14. ^{13}C NMR spectrum of AOAP.

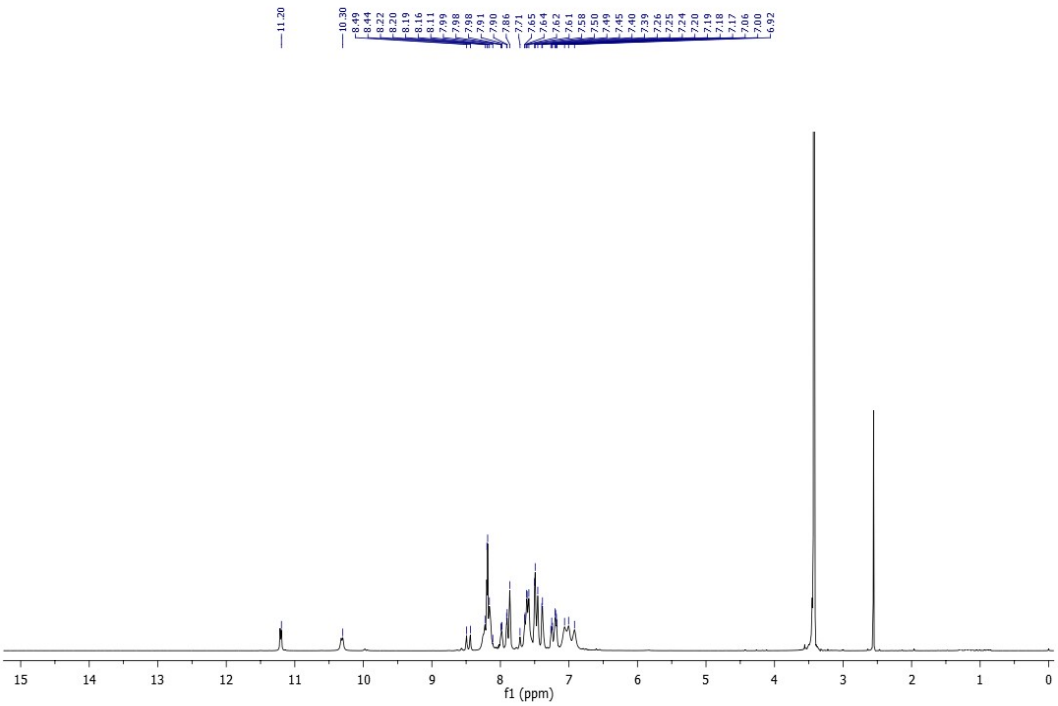

Figure S15. ^{1}H NMR spectrum of [Zn(AOBP)$_2$].

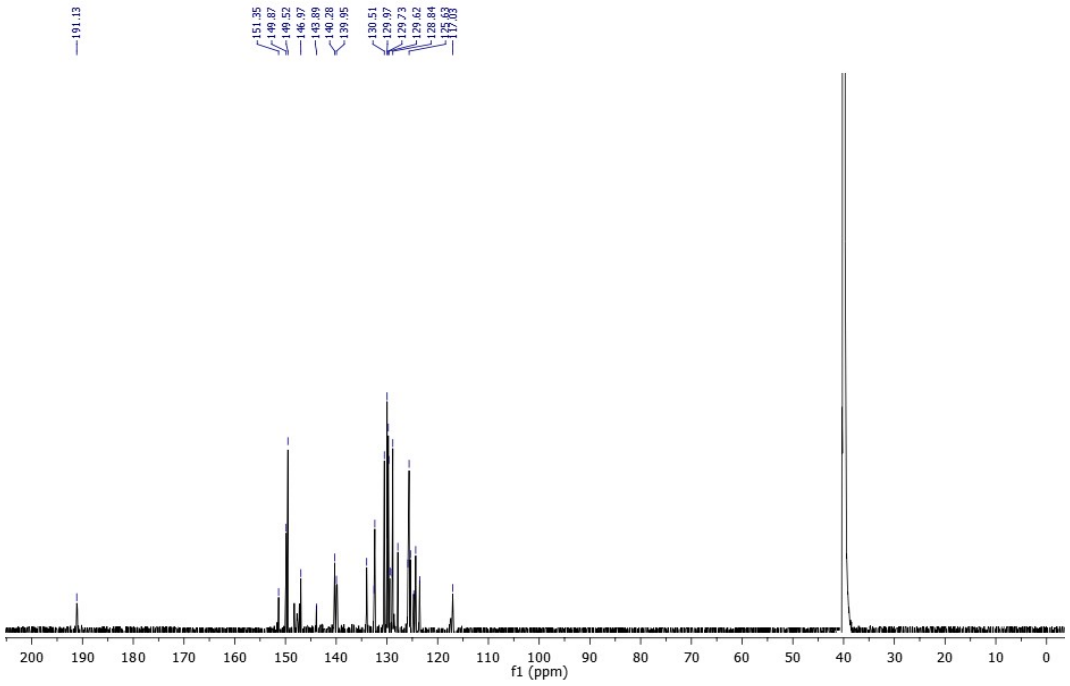

Figure S16. ^{13}C NMR spectrum of [Zn(AOBP)$_2$].

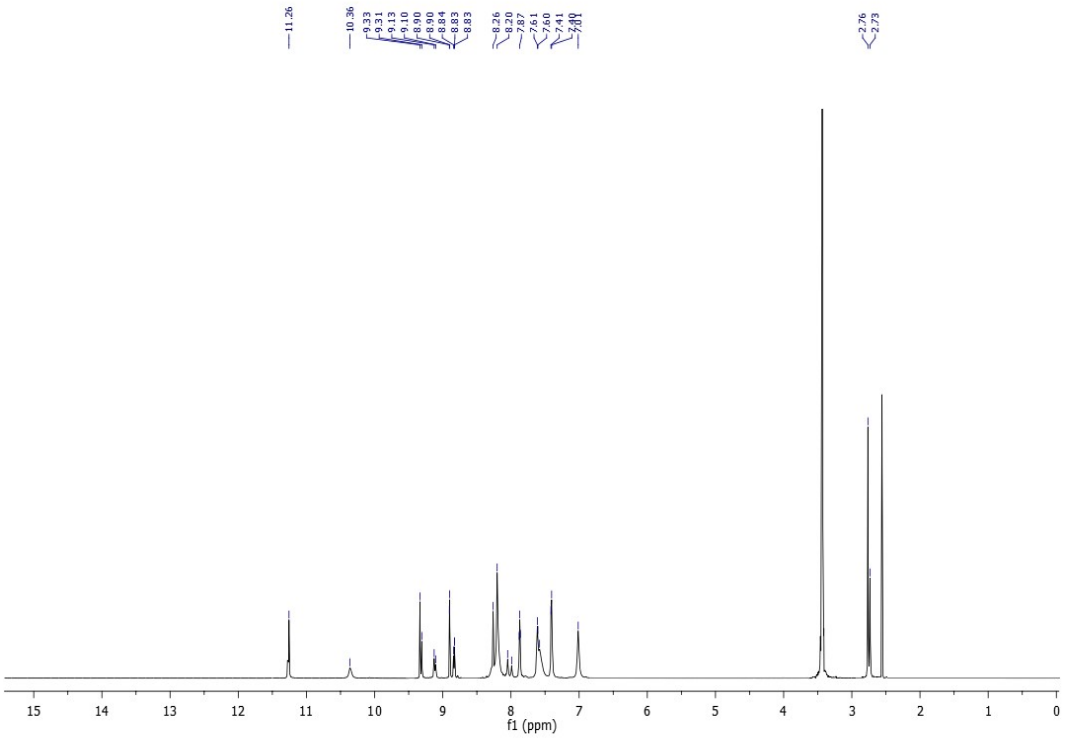

Figure S17. ^{1}H NMR spectrum of [Zn(AOAPZ)$_2$].

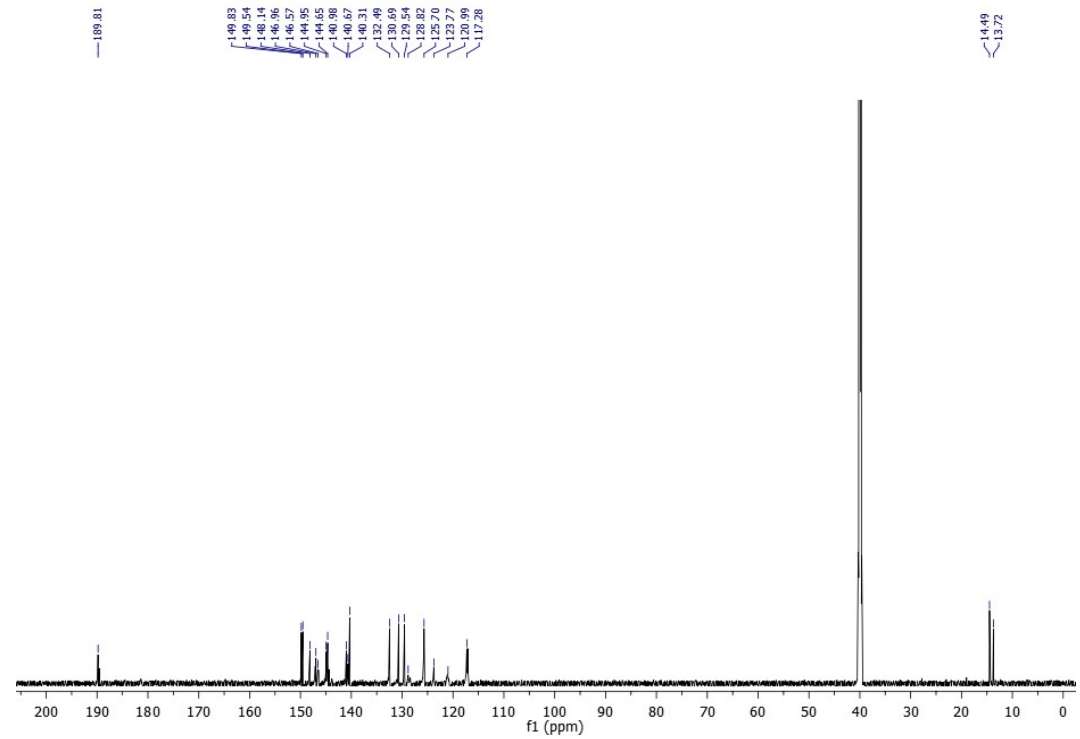

Figure S18. ^{13}C NMR spectrum of [Zn(AOAPZ)$_2$].

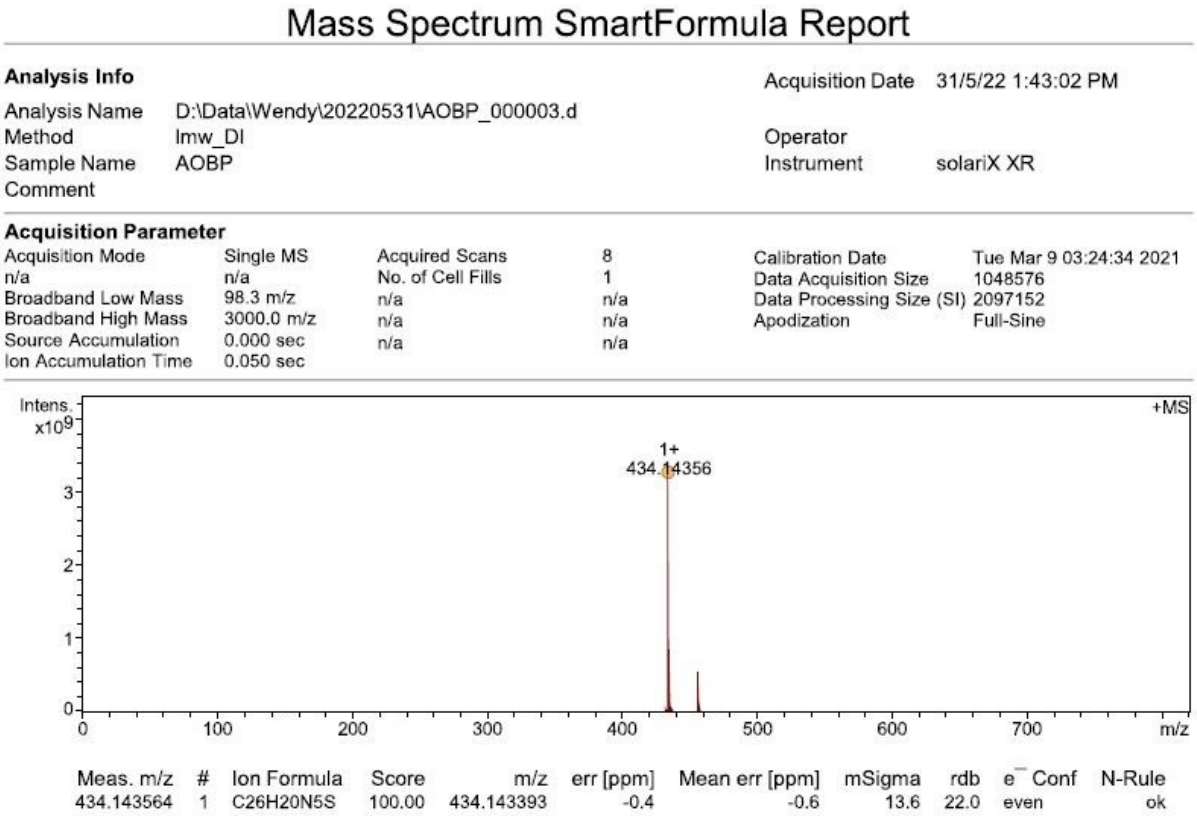

Figure S19. HR-MS spectrum of AOBP.

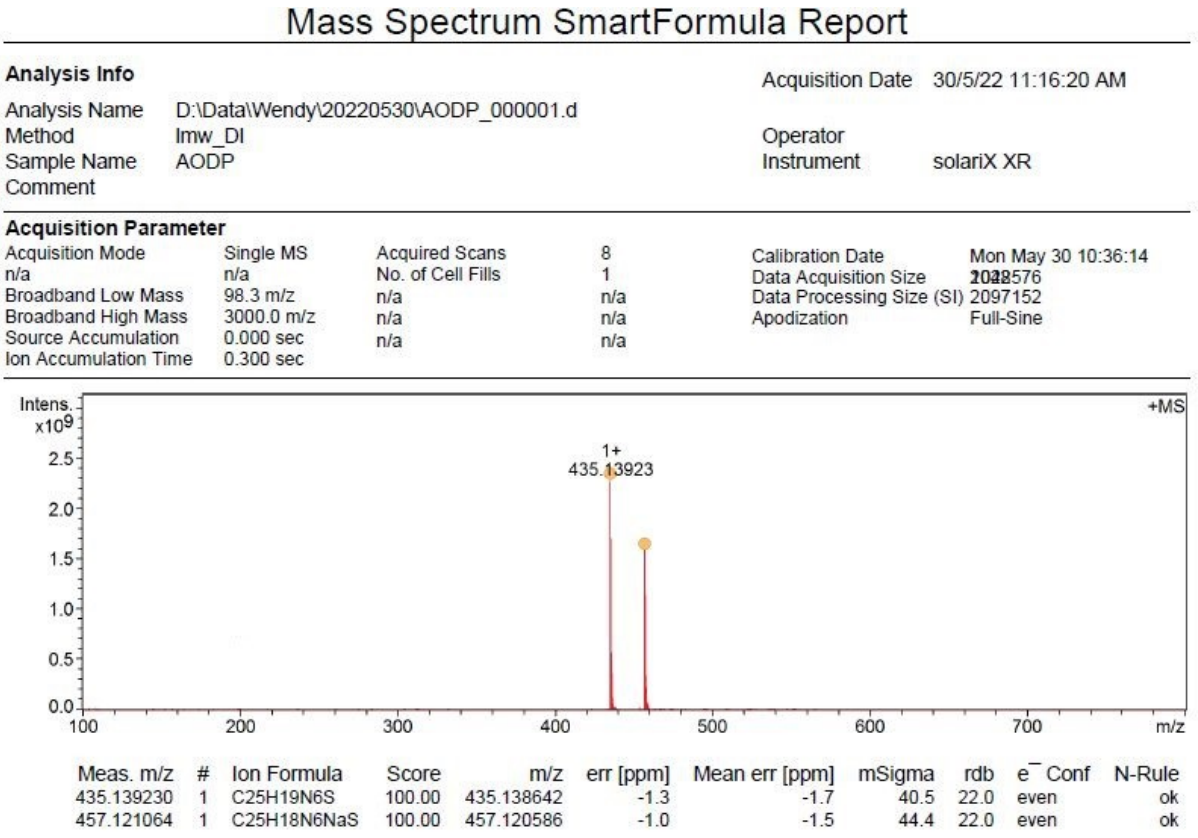

Figure S20. HR-MS spectrum of AODP

High Resolution Mass Spectrum

Analysis Info

Analysis Name	D:\Data\Wendy\20220912\AOAP2.d		
Method	DirectInfusion_2018_pos.m	Acquisition Date	10/12/2022 10:32:07 AM
Sample Name	AOAP2	Instrument	maXis II ETD 1823391.22321
Comment			

+MS, 0.3min #13-18

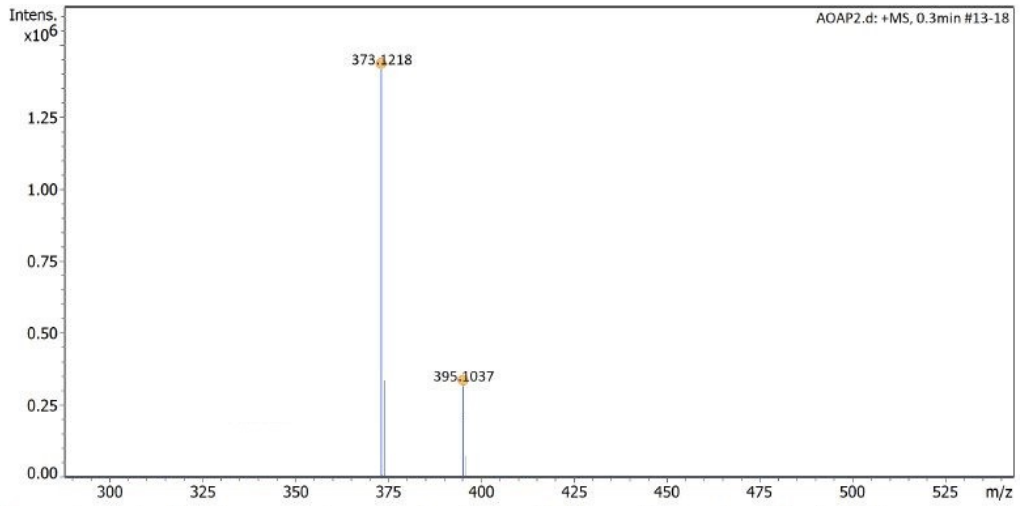

Meas. m/z	#	Ion Formula	m/z	err [ppm]	mSigma	# mSigma	Score	rdb	e⁻ Conf	N-Rule
373.1218	1	C20H17N6S	373.1230	3.2	12.2	1	100.00	18.0	even	ok
395.1037	1	C20H16N6NaS	395.1049	3.1	17.0	1	100.00	18.0	even	ok

Figure S21. HR-MS spectrum of AOAPZ

High Resolution Mass Spectrum

Analysis Info

Analysis Name	D:\Data\Wendy\20220912\AOAP000001.d		
Method	DirectInfusion_2018_pos.m	Acquisition Date	10/12/2022 11:04:48 AM
Sample Name	AOAP	Instrument	maXis II ETD 1823391.22321
Comment			

+MS, 0.5min #29

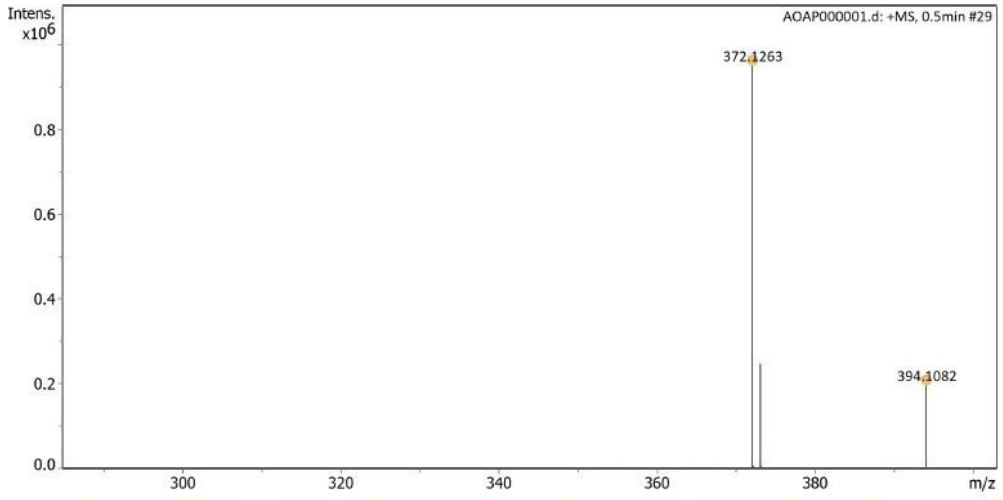

Meas. m/z	#	Ion Formula	m/z	err [ppm]	mSigma	# mSigma	Score	rdb	e⁻ Conf	N-Rule
372.1263	1	C21H18N5S	372.1277	3.9	3.8	1	100.00	18.0	even	ok
394.1082	1	C21H17N5NaS	394.1097	3.8	17.5	1	100.00	18.0	even	ok

Figure S22. HR-MS spectrum of AOAP

References

1. M. Whitnall, J. Howard, P. Ponka and D. R. Richardson, *Proc. Natl. Acad. Sci.*, 2006, **103**, 14901-14906.

2. A. E. Stacy, D. Palanimuthu, P. V. Bernhardt, D. S. Kalinowski, P. J. Jansson and D. R. Richardson, *J. Med. Chem.*, 2016, **59**, 4965-4984.

3. J. Yuan, D. B. Lovejoy and D. R. Richardson, *Blood*, 2004, **104**, 1450-1458.

4. M. Dharmasivam, B. Kaya, T. Wijesinghe, M. Gholam Azad, M. A. Gonzálvez, M. Hussaini, J. Chekmarev, P. V. Bernhardt and D. R. Richardson, *J. Med. Chem.*, 2023, **66**, 1426-1453.

5. D. B. Lovejoy, D. M. Sharp, N. Seebacher, P. Obeidy, T. Prichard, C. Stefani, M. T. Basha, P. C. Sharpe, P. J. Jansson and D. S. Kalinowski, *J. Med. Chem.*, 2012, **55**, 7230-7244.

6. S. Gharami, K. Aich, L. Patra and T. K. Mondal, *New J. Chem.*, 2018, **42**, 8646-8652.

7. F. Grases, F. Garcia-Sanchez and M. Valcarcel, *Anal. Chim. Acta*, 1980, **119**, 359-365.

8. J. A. Gilleran, X. Yu, A. J. Blayney, A. F. Bencivenga, B. Na, D. J. Augeri, A. R. Blanden, S. D. Kimball, S. N. Loh and J. Y. Roberge, *J. Med. Chem.*, 2021, **64**, 2024-2045.

9. L.-l. Liang, M. Li, J.-c. Liu and Y. Wei, *Acta Crystallogr. Sect. E Struct. Rep.*, 2012, **68**, m710-m710.

10. A. Danihel, S. Böhm and T. Busová, *Chem Pap-Chem Zvesti*, 2001, **55**, 113-117.

11. G. M. Sheldrick, *Acta Crystallogr. C Struct. Chem.*, 2015, **71**, 3-8.

12. D. Richardson, E. Tran and P. Ponka, *Blood*, 1995, **86**, 4295–4306.

13. D. Richardson and K. Milnes, *Blood*, 1997, **89**, 3025-3038.

14. C. C. Uphoff and H. G. Drexler, *In Vitro Cell. Dev. Biol.*, 2002, **38**, 79-85.

15. D. S. Kalinowski, Y. Yu, P. C. Sharpe, M. Islam, Y.-T. Liao, D. B. Lovejoy, N. Kumar, P. V. Bernhardt and D. R. Richardson, *J. Med. Chem.*, 2007, **50**, 3716-3729.

16. C. Stefani, P. J. Jansson, E. Gutierrez, P. V. Bernhardt, D. R. Richardson and D. S. Kalinowski, *J. Med. Chem.*, 2013, **56**, 357-370.

17. D. R. Richardson, D. S. Kalinowski, V. Richardson, P. C. Sharpe, D. B. Lovejoy, M. Islam and P. V. Bernhardt, *J. Med. Chem.*, 2009, **52**, 1459-1470.

18. C. Stefani, G. Punnia-Moorthy, D. B. Lovejoy, P. J. Jansson, D. S. Kalinowski, P. C. Sharpe, P. V. Bernhardt and D. R. Richardson, *J. Med. Chem.*, 2011, **54**, 6936-6948.

19. J. Gao and D. R. Richardson, *Blood*, 2001, **98**, 842-850.

20. M. Gholam Azad, M. Hussaini, T. M. Russell, V. Richardson, B. Kaya, M. Dharmasivam and D. R. Richardson, *J. Biol. Chem.*, 2024, DOI: https://doi.org/10.1016/j.jbc.2024.107417.

21. S. Bolte and F. P. Cordelières, *J. Microsc.*, 2006, **224**, 213-232.

22. A. E. Stacy, D. Palanimuthu, P. V. Bernhardt, D. S. Kalinowski, P. J. Jansson and D. R. Richardson, *J. Med. Chem.*, 2016, **59**, 4965-4984.

23. J. Cáceres, J. Robinson-Duggon, A. Tapia, C. Paiva, M. Gomez, C. Bohne and D. Fuentealba, *Phys. Chem. Chem. Phys.*, 2017, **19**, 2574-2582.

24. T. P. Wijesinghe, B. Kaya, M. A. Gonzálvez, J. R. Harmer, M. Gholam Azad, P. V. Bernhardt, M. Dharmasivam and D. R. Richardson, *J. Med. Chem.*, 2023, **66**, 15453-15476.

25. P. V. Bernhardt, P. C. Sharpe, M. Islam, D. B. Lovejoy, D. S. Kalinowski and D. R. Richardson, *J. Med. Chem.*, 2009, **52**, 407-415.

26. D. Kovala-Demertzi, P. N. Yadav, J. Wiecek, S. Skoulika, T. Varadinova and M. A. Demertzis, *J. Inorg. Biochem.*, 2006, **100**, 1558-1567.

27. M. X. Li, C. L. Chen, D. Zhang, J. Y. Niu and B. S. Ji, *Eur. J. Med. Chem.*, 2010, **45**, 3169-3177.

28. T. P. Stanojkovic, D. Kovala-Demertzi, A. Primikyri, I. Garcia-Santos, A. Castineiras, Z. Juranic and M. A. Demertzis, *J. Inorg. Biochem.*, 2010, **104**, 467-476.

29. A. Jiménez-Pérez, S. Fernández-Fariña, R. Pedrido and J. García-Tojal, *J. Biol. Inorg. Chem.*, 2024, **29**, 3-31.

30. R. Gil-Garcia, R. Fraile, B. Donnadieu, G. Madariaga, V. Januskaitis, J. Rovira, L. Gonzalez, J. Borras, F. J. Arnáiz and J. Garcia-Tojal, *New J. Chem.*, 2013, **37**, 3568-3580.